NeuroImage: Clinical 38 (2023) 103407

Contents lists available at ScienceDirect

NeuroImage: Clinical

journal homepage: www.elsevier.com/locate/ynicl

Degradation of EEG microstates patterns in subjective cognitive decline and mild cognitive impairment: Early biomarkers along the Alzheimer's Disease continuum?

Michael Lassi [a], Carlo Fabbiani [b], Salvatore Mazzeo [b,c], Rachele Burali [b], Alberto Arturo Vergani [a], Giulia Giacomucci [c], Valentina Moschini [c], Carmen Morinelli [d], Filippo Emiliani [c], Maenia Scarpino [b], Silvia Bagnoli [c], Assunta Ingannato [c], Benedetta Nacmias [b,c], Sonia Padiglioni [e], Silvestro Micera [a,f], Sandro Sorbi [b,c], Antonello Grippo [b,1], Valentina Bessi [c,1], Alberto Mazzoni [a,1,*]

[a] The BioRobotics Institute and Department of Excellence in Robotics and AI, Sant'Anna School of Advanced Studies, viale Rinaldo Piaggio 34, 56025 Pisa, Italy
[b] IRCCS Fondazione Don Carlo Gnocchi, via di Scandicci, 269, 50143 Florence, Italy
[c] Department of Neuroscience, Psychology, Drug Research and Child Health, University of Florence, Careggi University Hospital, viale Gaetano Pieraccini, 6, 50139 Florence, Italy
[d] Dipartimento Neuromuscolo-scheletrico e degli organi di senso, Careggi University Hospital, 50134 Florence, Italy
[e] Regional Referral Centre for Relational Criticalities - Tuscany Region, 50139 Florence, Italy
[f] Bertarelli Foundation Chair in Translational Neuroengineering, Centre for Neuroprosthetics and Institute of Bioengineering, School of Engineering, École Polytechnique Fédérale de Lausanne (EPFL), 1015 Lausanne, Switzerland

ARTICLE INFO

Keywords:
Subjective cognitive decline
Mild cognitive impairment
EEG
Microstates
Alzheimer's Disease

ABSTRACT

Alzheimer's disease (AD) pathological changes may begin up to decades earlier than the appearance of the first symptoms of cognitive decline. Subjective cognitive decline (SCD) could be the first pre-clinical sign of possible AD, which might be followed by mild cognitive impairment (MCI), the initial stage of clinical cognitive decline. However, the neural correlates of these prodromic stages are not completely clear yet. Recent studies suggest that EEG analysis tools characterizing the cortical activity as a whole, such as microstates and cortical regions connectivity, might support a characterization of SCD and MCI conditions. Here we test this approach by performing a broad set of analyses to identify the prominent EEG markers differentiating SCD (n = 57), MCI (n = 46) and healthy control subjects (HC, n = 19). We found that the salient differences were in the temporal structure of the microstates patterns, with MCI being associated with less complex sequences due to the altered transition probability, frequency and duration of canonic microstate C. Spectral content of EEG, network connectivity, and spatial arrangement of microstates were instead largely similar in the three groups. Interestingly, comparing properties of EEG microstates in different cerebrospinal fluid (CSF) biomarkers profiles, we found that canonic microstate C displayed significant differences in topography in AD-like profile. These results show that the progression of dementia might be associated with a degradation of the cortical organization captured by microstates analysis, and that this leads to altered transitions between cortical states. Overall, our approach paves the way for the use of non-invasive EEG recordings in the identification of possible biomarkers of progression to AD from its prodromal states.

Abbreviations: SCD, Subjective Cognitive Decline; MCI, Mild Cognitive Impairment; AD, Alzheimer's Disease; HC, Healthy Controls; CSF, Cerebrospinal fluid; LZ, Lempel-Ziv; GFP, Global Field Power; GMD, Global Map Dissimilarity; TANOVA, Topographical Analysis of Variance.

* Corresponding author.
E-mail address: alberto.mazzoni@santannapisa.it (A. Mazzoni).
[1] these authors share same senior author contribution.

https://doi.org/10.1016/j.nicl.2023.103407
Received 6 October 2022; Received in revised form 29 March 2023; Accepted 14 April 2023
Available online 19 April 2023

1. Introduction

Alzheimer's Disease (AD) is the end-point of a continuum, in which the pathological changes may begin even decades earlier than the appearance of the first symptoms (Sperling et al., 2011). Anticipating the diagnosis of AD is essential to develop early intervention and coordinated care plans (Dubois et al., 2016). Furthermore, the future advent of disease-modifying treatments for dementia (Cummings et al., 2007) makes the identification of reliable and easily accessible tools to predict AD an urgent priority. The AD continuum has been separated into preclinical stages, in which no objective cognitive decline is observed, and clinical stages in which the neurodegeneration drives a loss in cognitive capacity (Sperling et al., 2011). Specifically, mild cognitive impairment (MCI) is defined as the state of objective cognitive decline as measured by clinical and cognitive scales, without an impact on the activities of daily living (Petersen, 2004). In the last decade, increased interest has also been focused on the subjective cognitive decline (SCD) condition. SCD is the self-concerned experience of reduced cognitive function, while maintaining normal scores on standardized cognitive tests (Jessen et al., 2014). There is some evidence that SCD may be a prelude to AD: while SCD has been described as a heterogenous condition, with many possible longitudinal outcomes, individuals having SCD are more likely to progress to dementia than the rest of the elderly population (Jessen et al., 2020). Specifically, the SCD population displays a higher risk of developing MCI and AD dementia (Perrotin et al., 2012; Stewart et al., 2011). Hence, SCD might represent a target population for disease-modifying therapies to preserve cognitive function and psychological well-being (Bhome et al., 2018).

Current diagnosis of AD largely relies on the use of biomarkers that are either costly to acquire or invasive, such as PET neuroimaging or cerebrospinal fluid markers (CSF) (Jack et al., 2018). These biomarkers, while being able to properly differentiate AD from other forms of dementia early in the degeneration continuum, are not suitable for the screening of large populations. In this sense, EEG may be an excellent device to screen the SCD population, as it is a relatively cheap and totally non-invasive functional tool and it may even be a complementary tool to other dementia biomarkers (Ferreira et al., 2016). Several studies have focused on identifying quantitative EEG markers to diagnose AD, comparing it to healthy elderly controls (Cassani et al., 2018). Here, we will focus mostly on the resting-state EEG paradigm, as it is the most widely available EEG tool in the clinical setting. A large number of studies investigated quantitative EEG markers of AD, and they can mostly be distinguished into the following categories: spectral markers, connectivity and network metrics, complexity measures and microstates (Maestú et al., 2019). Generally, as regards power spectrum, a slowing of the oscillations in the EEG activity is observed, with a decrease of higher frequency activity (alpha and beta bands) or increase of low-frequency power (delta and theta bands) in AD and MCI groups compared to healthy controls (Fonseca et al., 2011; Jelic et al., 1996; Kim et al., 2012). Complementarily to that, several studies highlighted a reduction in complexity of the EEG signal throughout the development of dementia (Kulkarni et al., 2017; Shumbayawonda et al., 2020; Tait et al., 2020). Another interesting perspective on EEG alterations is provided by connectivity studies looking for patterns of covariations in EEG sensors' or sources' signals. Several metrics can be used for estimating functional connectivity among areas, such as coherence, linear lagged connectivity and imaginary coherence. The latter is often used, as it is rather simple to implement and it reduces the effect of possible spurious connections due to volume conduction (Bastos and Schoffelen, 2016; Nolte et al., 2004). Its use is widely accepted in the analysis of neurological disorders, including AD studies as well (Lam and Shafi, 2022). Connectivity studies in AD generally highlight a decrease in the degree of connectivity between brain areas, specifically in the higher frequency bands (for spectral-related connectivity measures) (Babiloni et al., 2018b; Besthorn et al., 1994; Meghdadi et al., 2021; Smailovic et al., 2020). Analyzing the functional connectome obtained by EEG with a network theory approach leads to single measures capturing global properties of the whole network. Some prominent results in this context regard the disruption of the small-world property in the AD continuum (Rossini et al., 2020; Vecchio et al., 2018).

Finally, microstates are recurrent scalp topographies in the EEG signal, found to be quasi-stable over periods of 60–120 ms (Michel and Koenig, 2018). Different clustering techniques, such as k-means and hierarchical clustering, can be used to identify the most common topographies in the EEG signal. At rest, four canonical microstates are typically identified (named A to D). In this view, the EEG signal can be represented as a sequence of these microstates, in which only one of them is active at each time-point (winner-takes-all approach). Starting from this discrete sequence, several metrics can be extracted (Koenig et al., 2014), both related to the dynamics of microstates patterns (duration, coverage, frequency of occurrence, transition probabilities) and to their topographies. Microstates have been shown to be related to different active resting-state networks and to have functional significance (Milz et al., 2016). Many studies highlighted how microstates patterns vary in pathological conditions (da Cruz et al., 2020; Murphy et al., 2020; Nishida et al., 2013; Zappasodi et al., 2017), and demonstrated their use as markers of the pathology. Microstate analysis have also been applied to extract information about AD and dementia (Dierks et al., 1997; Grieder et al., 2016; Musaeus et al., 2020; Nishida et al., 2013; Tait et al., 2020).

Of note, all the afore-mentioned studies have focused on MCI, AD and the transition from the former to the latter. To the best of our knowledge only few studies described quantitative EEG changes in SCD subjects, mostly focusing on spectral analyses (e.g., (Alexander et al., 2006; Babiloni et al., 2010; Jeong et al., 2021; Smailovic et al., 2018)) and used spectral markers to predict the converters to dementia (Engedal et al., 2020). Other studies investigated the connectivity patterns and network metrics in EEG in the SCD condition (Lazarou et al., 2020, 2019; López-Sanz et al., 2017; Smailovic et al., 2018). Finally, one study investigated the differences in the topography of microstates among SCD, MCI and AD conditions (Smailovic et al., 2019).

In the present study, we aimed to assess the efficacy of a broad set of the afore-mentioned EEG features in discriminating between SCD and MCI data first, and then in discriminating AD CSF biomarker profiles.

2. Methods

2.1. Participants

The "PRedicting the EVolution of SubjectIvE Cognitive Decline to Alzheimer's Disease With machine learning (PREVIEW)" project (Mazzeo et al., 2023) is an ongoing prospective cohort study started in October 2020 and including consecutive patients with SCD and MCI who self-referred to the Regional Reference Center for Alzheimer's Disease and Cognitive Disorders of Careggi Hospital, Florence. All patients underwent a comprehensive family and clinical history, neurological examination, extensive neuropsychological investigation, estimation of premorbid intelligence, and assessment of depression. The following inclusion criteria were adopted: complaint of cognitive decline with a duration of $\geq$ 6 months; Mini Mental State Examination (MMSE) score $>$24, corrected for age and education; normal functioning on the Activities of Daily Living (ADL) and the Instrumental Activities of Daily Living (IADL) scales (Lawton and Brody, 1969); unsatisfied criteria for AD diagnosis according to National Institute on Aging-Alzheimer's Association (NIA-AA) criteria (McKhann et al., 2011).

Exclusion criteria were: history of head injury, current neurological and/or systemic disease, symptoms of psychosis, major depression, alcoholism, or other substance abuse; complete data loss of patients' follow-up; use of any medication with known effects on EEG oscillations, such as benzodiazepines or antiepileptic drugs.

A total of 113 patients were considered. Based on clinical, neurological, and neuropsychological examination, we excluded four patients

as they presented other diseases (one patient had obstructive sleep apnea syndrome, one patient had bladder cancer, one patient was diagnosed with major depression, one patient died for unknown causes); six patients refused to underwent EEG. Therefore, we included 103 patients. They were classified as 57 SCD, according to Subjective Cognitive Decline Initiative (SCD-I) Working Group (Jessen et al., 2014) criteria, and 46 MCI based on NIA-AA criteria (Albert et al., 2011). Additionally, 19 volunteer healthy control subjects (HC), aged 55 to 75 years, were recruited to assess resting-state EEG. Each subject underwent a clinical and family history, a basic neuropsychological testing through MMSE and a general and neurological examination. Exclusion criteria, in addition to those used for SCD or MCI subjects, were: concern about cognitive decline or memory loss, familiarity for Alzheimer's disease, MMSE score < 27 (corrected for age and education).

Summary demographics of each group are reported in Table 1.

Resting-state EEG data was collected from patients meeting inclusion criteria at the IRCCS Don Gnocchi (Florence, Italy). EEG was collected from patients resting on a chair in a comfortable position, using the 64-channels Galileo-NT system (E.B. Neuro S.p.a.). Sensors location followed the extended 10/20 system (Oostenveld and Praamstra, 2001). Unipolar signals were recorded at a sampling rate of 512 Hz. EEG recording began with a 10-minute eyes-closed registration followed by an alternance of 3 min eyes-open and 3 min eyes closed, repeated twice, as per indications of the International Federation of Clinical Neurophysiology (Babiloni et al., 2020). During the eyes-closed condition, the subjects were asked to sit in a comfortable position, with eyes-closed and to relax in a state of mind-wandering (with no goal-oriented mental activity) (Babiloni et al., 2020). The first phase of the recording was designed to be longer in order to obtain a reliable resting-state recording at eyes closed. During the EEG acquisition, impedance of the electrodes was monitored to be lower than 10 kOhm. All electrodes' impedances were balanced to be in the range between 7 and 10 kOhm. Whenever the impedance went over the threshold, the electrode was re-adjusted and the portion of signal related to that time was removed. Only the eyes-closed portions of the signal were used for subsequent analyses.

A subset (48.5%) of the cohort (n = 50, SCD = 30, MCI = 20) additionally underwent lumbar puncture examination to obtain CSF biomarkers. The CSF samples collected by lumbar puncture were immediately centrifuged and stored at −80 °C until performing the analysis. $A\beta_{42}$, $A\beta_{42}/A\beta_{40}$ ratio, t-tau, and p-tau have been measured using a chemiluminescent enzyme immunoassay (CLEIA) analyzer LUMIPULSE G600 (Fujirebio, Tokyo, Japan) (Alcolea et al., 2019). Cut-off values for CSF were determined following Fujirebio guidelines (Diagnostic sensitivity and specificity using clinical diagnosis and follow-up golden standard, November 19th, 2018): $A\beta_{42} > 670$ pg/ml, $A\beta_{42}/A\beta_{40}$ ratio > 0.062, t-tau < 400 pg/ml and p-tau < 60 pg/ml. Patients were rated according to the A/T(N) system (Jack et al., 2016): A^+ or A^- if $A\beta_{42}$ or $A\beta_{42}/A\beta_{40}$ were lower or higher than cut-off values respectively; T^+ or T^- and N^+ or N^- if CSF p-tau and t-tau concentrations were higher or lower than cut-off values. We defined patients as: carriers of AD pathology when A + was associated with either T + or N+ (A+/T+/N+, A+/T+/N− or A+/T−/N +); non-carriers of AD pathology when they were classified as A− (regardless of T and N classification) or as A+/T−/N−.

All subjects were recruited in accordance with the Declaration of Helsinki and with the ethical standards of the Committee on Human Experimentation of Careggi University Hospital (Florence, Italy). The study was approved by the local Institutional Review Board (reference 15691oss). All participants in this study signed an informed consent, agreeing to participate and to share the results deriving from their data.

Table 1
Demographics of recruited subjects. Each value is indicated as mean followed, when possible, by the standard deviation in parenthesis.

	HC	SCD	MCI
Sex	8F 11 M	41F 16 M	29F 17 M
Age	64.29 (4.77)	67.19 (9.30)	74.26 (8.66)
Age at onset of symptoms	–	54.89 (8.78)	61.67 (9.81)
MMSE	29.06 (1.13)	28.07 (2.18)	26.82 (2.23)
TIB	–	108.82 (18.44)	107.73 (9.69)
Years of Education	15.64 (3.62)	12.61 (3.76)	10.02 (3.85)
History of AD in the family	–	38	27

MMSE: Mini Mental State Examination.
TIB: Test Intelligenza Breve (Italian Brief Intelligence Test).

2.2. EEG preprocessing

In order to remove electrophysiological and non-electrophysiological artifacts from the raw signals, we used a custom preprocessing pipeline written in Matlab with the use of the EEGLAB toolbox functions (Delorme and Makeig, 2004). The pipeline consisted of two main steps: the PREP pipeline (Bigdely-Shamlo et al., 2015), followed by ICA removal of artifactual components (Delorme et al., 2007).

The first step of preprocessing included the use of the PREP pipeline, which performs several routines automatically, allowing to obtain robust average re-referenced signals. Initially, PREP high-pass filters signals of all channels, by means of a Hamming windowed FIR filter (using EEGLAB's *pop_eegfiltnew* function) with a 1 Hz cut-off frequency. Line noise at 50 Hz and its harmonics were removed by using the CleanLine EEGLAB plugin. Noisy channels, i.e., those channels having abnormal and/or uncorrelated activity compared to others were removed by using PREP noisy channel subroutine, which performs the bad channel selection by combining an ensemble of methods: the deviation criterion, the correlation criterion, the noisiness criterion, and the predictability criterion. Remaining channels activity was used to estimate a robust average reference, based on robust statistics such as the median and interquartile range. Finally, removed channels were interpolated, by means of spherical interpolation. The obtained re-referenced and filtered signals were then subjected to the second preprocessing step.

Independent components were extracted by using the Infomax ICA algorithm (Bell and Sejnowski, 1995), as implemented in *binica* EEGLAB routine. A semi-automated procedure was then used to distinguish between brain-related components and artifactual ones. We used ICLabel (Pion-Tonachini et al., 2019) to classify automatically independent components into brain or artifactual components (line noise, muscle, eye, channel noise, heart, "other") based on a neural network trained on crowd-sourced data. ICLabel returns the probability of each component to belong to one of the above-mentioned classes. We then used DIPFIT to perform a single dipole fitting of the independent component map onto a template brain (MNI-152 atlas). Given that brain components should be dipolar (Delorme et al., 2012), a high residual variance of the fitted dipole should indicate a low probability of the component being brain-related. Hence, components labeled by ICLabel as "brain" with a confidence higher than a threshold (we used 75%) and having fitted dipole residual variance lower than another threshold (we used 20%) were retained in the final signals. Noise components with high confidence and high dipole residual variance were instead automatically removed from the ICs list. All the remaining components were inspected visually and flagged either as brain or non-brain depending on their power spectra profiles and time-courses. Channel-level signals were finally reconstructed from the reduced IC space, only including brain-related sources. Finally, we performed a visual inspection of the cleaned signals, to remove possible remaining artifacts (e.g., temporally localized muscle activity not removed by the ICA procedure).

A summary of the subsequent methodology to extract EEG features is displayed in Fig. 1.

2.3. PSD metrics

We computed an estimate of the power spectral density (PSD) of the

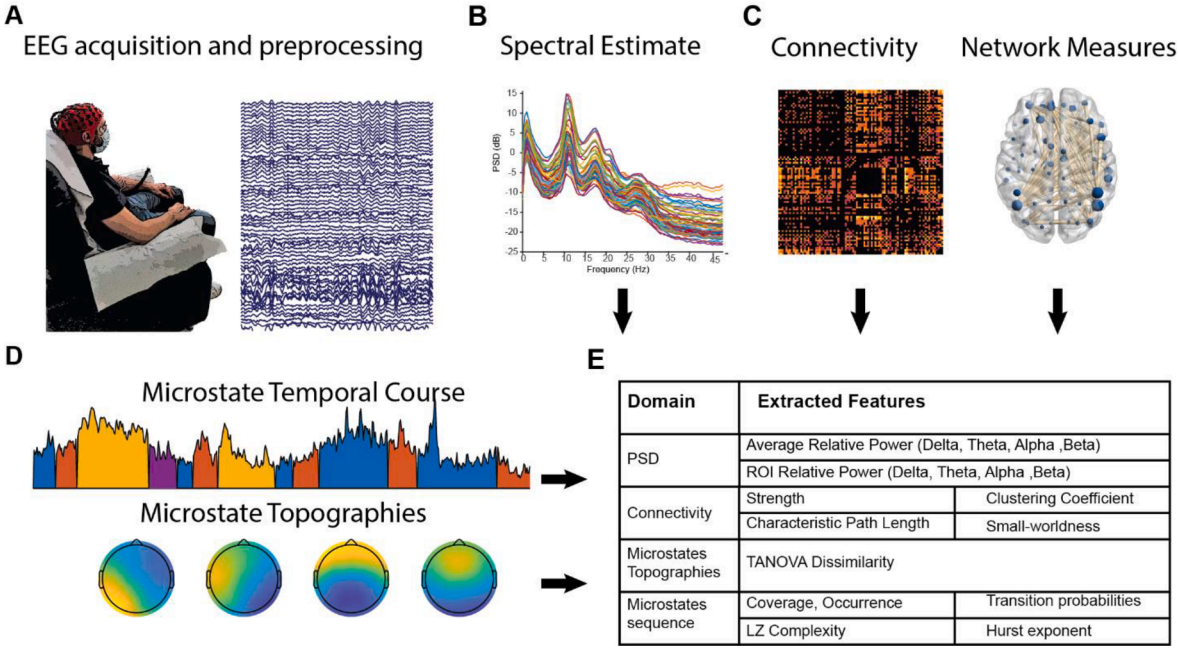

Domain	Extracted Features	
PSD	Average Relative Power (Delta, Theta, Alpha ,Beta)	
	ROI Relative Power (Delta, Theta, Alpha ,Beta)	
Connectivity	Strength	Clustering Coefficient
	Characteristic Path Length	Small-worldness
Microstates Topographies	TANOVA Dissimilarity	
Microstates sequence	Coverage, Occurrence	Transition probabilities
	LZ Complexity	Hurst exponent

Fig. 1. Methodological approach. (A) The eyes-closed EEG signal is acquired and preprocessed by means of the PREP pipeline (Bigdely-Shamlo et al., 2015) and ICA artifact removal techniques. (B) Spectral densities are estimated with Welch Method from the cleaned signals in each subject, and band-wise relative power is computed in six regions of interest. (C) Signal is source-reconstructed, and a connectivity measure (imaginary part of coherency) is computed. The cortical dipoles are parcellated into anatomical ROIs and the resulting connectivity network is globally evaluated by means of graph-theoretical metrics. (D) EEG signals are clustered into four subject-specific topographies and their temporal sequence is computed. Both topographical and temporal features are extracted from microstates activity. (E) The computed methods are tested statistically to check for differences among groups.

signal in each of the recorded channels. We applied the Welch's method (averaged periodogram) on 5 s continuous windows of EEG signals, using Hanning windows with no overlap. We then divided the spectrum in four canonical frequency bands, namely: delta (1–4 Hz), theta (4–8 Hz), alpha (8–13 Hz) and beta (13–30 Hz). For each band, the absolute power was first computed by using the trapezoid integration method (Matlab *trapz* function), and then normalized to the total power in the frequency range 1–48 Hz (upper limit set to avoid possible residual line noise activity). The average power is finally computed as the mean power across all EEG channels. We finally divided the scalp in six regions of interest (ROIs) (Fanciullacci et al., 2017): frontal right (Fp2, AF4, AF8, F2, F4, F6, F8) frontal left (Fp1, AF3, AF7, F1, F3, F5, F7), central right (FC2, FC4, FC6, FT8, C2, C4, C6, T4, CP2, CP4, CP6), central left (FC1,FC3, FC5, FT7, C1, C3, C5, T3, CP1, CP3, CP5), occipital right (P2, P4, P6, T6, PO8, PO4, O2) and occipital left (P1, P3, P5, T5, PO7, PO3, O1). ROI power was computed as the average relative power from channels belonging to each ROI. The same analysis was applied to the absolute power of the EEG signals in the six ROIs and four frequency bands.

2.4. Connectivity and network metrics

From the preprocessed sensors' level data, an estimate of cortical sources activity was obtained by means of the eLORETA method (Pascual-Marqui, 2007), implemented in the Fieldtrip Matlab toolbox (Oostenveld et al., 2011). No subject-specific head models were used in the reconstruction process, as structural MRI images were not available for all subjects. We instead used a 3D-mesh model, constituted of tetrahedrical elements, reconstructed from the ICBM152 template and available in Fieldtrip, prepared for Boundary Elements Method (Oostenveld et al., 2003). The template head model is composed of three-layer tissues (skin, skull, brain), each with a different value of electrical conductivity. Using a common template head model for all subjects allowed direct comparison of the achieved results. Moreover, it has been shown that reconstruction accuracy is comparable between template-models and subject-specific models (Douw et al., 2018). The source model used for the reconstruction was a canonical cortical sheet with 5124 vertices (dipoles), located at the middle cortical sheet of a standard MNI brain. This template source model was taken from the SPM8 software, as available in the Fieldtrip toolbox.

eLORETA solves the inverse problem of source reconstruction by imposing the solution to be a smooth, low-resolution distribution of cortical activations. We used as smoothing factor lambda = 0.03. Since the measure of connectivity of choice was based on spectral coherence (as described below) we decided to solve the source reconstruction problem directly on the Fourier-transformed data obtained during the PSD analysis, as to obtain directly the spectral representation of the sources. The three-dimensional dipole moments were summarized by the activity along the direction of maximum activation by computing the SVD decomposition and retaining only the first component. Once source activity was reconstructed, dipoles' locations were parcellated into an atlas, by computing the average activation of the dipoles in each region of interest (ROI). We used as reference atlas the Automated Anatomical Labeling atlas (v3) (Tzourio-Mazoyer et al., 2002), and only considered the cortical regions inside the atlas. The resulting included regions are reported in Supplementary Table 1.

Spectra were divided in the same four bands as in the PSD analysis.

To measure the level of connectivity between pairs of brain regions, we used the imaginary part of coherency metric (Nolte et al., 2004). For each pair of ROIs, we defined coherency as the normalized cross-spectrum:

$$C_{xy} = \frac{G_{xy}}{\sqrt{G_{xx}G_{yy}}}$$

G_{xy} is the cross-spectral densities of the two signals x(t) and y(t), while G_{xx} and G_{yy} are the respective spectral densities. The choice of imaginary coherence for estimating the connectivity among ROIs brings the benefit of avoiding overestimating connections due to the volume conduction effects, typical of EEG signals. In the computation of imaginary

coherence, zero-lag connectivity is neglected as it is entirely contained in the real part of the coherency metric (Bastos and Schoffelen, 2016).

To retain only sparse connections in the adjacency matrices, we adopted a pruning algorithm that maintained components connected. To achieve that, a percentile threshold was set to only retain connections having absolute value above the given percentile. The threshold was swept from 0 to 1 in steps of 0.01 and the connectedness of the network was checked at every iteration. The highest pruning threshold that resulted in no isolated components was selected, as to avoid issues in the subsequent computation of metrics (Rubinov and Sporns, 2010). Connectivity values below the threshold were set to zero. At the end of this process, for each subject, a symmetric matrix of weighted connections was computed.

From single-subject connectivity matrices in the four frequency bands defined above, we extracted several network metrics from the weighted undirected adjacency matrices. First, the average strength of the connectivity among pairs of ROIs was extracted (starting from the sparse adjacency matrix obtained by weight pruning). Average strength was simply defined the mean weight of non-zero connections. Then, the weighted clustering coefficient (C) and weighted characteristic path length (L) were computed as previously described (Vecchio et al., 2018).

Finally, the small-world coefficient was computed as:

$$\Omega = \frac{Lr}{L} - \frac{C}{Cl}$$

L and C are the previously computed weighted clustering coefficient and weighted characteristic path length, whereas Lr is the weighted characteristic path length of an equivalent random network and Cl is the weighted clustering coefficient of an equivalent lattice network. The equivalent networks were computed by randomizing (Maslov and Sneppen, 2002) and latticizing (Sporns and Zwi, 2004) weight coefficients but preserving the degree distribution of the adjacency matrix. The small-world coefficient Ω is 1 for a random network, −1 for a lattice and tends to 0 for networks following the small-world property. All network metrics were computed with the use of the Matlab Brain Connectivity Toolbox (Rubinov and Sporns, 2010).

2.5. Microstate extraction

Microstates are quasi-stable topographies observable in the EEG signals that remain stable over 60–120 ms before switching to another topography (Michel and Koenig, 2018). In order to capture which are the most recurrent EEG topographies in the signal, clustering techniques are used to map topographies to a limited set of primitives. While distinct clustering techniques may yield different results, it has been shown that these algorithms are information-theoretically invariant, hence indicating that extracted metrics are algorithm-independent (von Wegner et al., 2018). While several methodological approaches are possible, we decided to perform a two-step process in the identification of microstate maps, as to minimize possible bias in the results (Murphy et al., 2022). First, a set of microstate maps is extracted for each subject individually, then the subjects' microstate maps are averaged in grand-average maps. These maps are finally used as template for back-fitting microstates in the EEG signal.

In order to extract microstate maps for each subject individually, we first investigated which number of microstates was globally optimal. We extracted a first set of common microstates from the entirety of subjects (independent of conditions), by using the modified k-means algorithm (Pascual-Marqui et al., 1995). To reduce the computation time, 1000 global field power (GFP) peaks were randomly selected as input topographies to the clustering algorithm, as these maps should have the highest signal-to-noise ratio. GFP is defined (Murray et al., 2008) as the standard deviation of all electrodes' potentials at a given time:

$$GFP(t) = \sqrt{\frac{\sum_K (V_i(t) - V_{mean}(t))^2}{K}}$$

V_i is the potential at time t for the electrode i, V_{mean} is the average potential at time t, K is the total number of electrodes.

Topographies having GFP higher than two standard deviations from the mean were discarded from the selection process, as to avoid introducing noisy maps in the clustering algorithm. We ran the modified k-means (20 repetitions, 1000 max iterations) for each number of clusters from two to fifteen. For each iteration of the process, the found microstate maps were back-fitted to the entire preprocessed EEG signal, by assigning each topography from each time-point to the one minimizing the global map dissimilarity (GMD), namely the GFP of the difference between the two maps. The global explained variance was computed for each topography set. Finally, we selected the number of microstates for which the local improvement in the global explained variance metric was<5%. This number was found to be four, in accordance with what is reported in literature for resting-state signals, even using different criteria (Koenig et al., 2002; Michel and Koenig, 2018).

Once we determined the globally optimal number of maps, we fixed this number for all subsequent analyses, as to allow for easier comparison between groups. Subject-level microstate maps were computed by two-steps of processing. First, for each subject individually, a set of four maps was determined by applying again the modified k-means clustering algorithm on GFP peaks' topographies. To speed-up the computation for each subject a subset of $3*10^4$ GFP peaks were randomly selected as input to the clustering algorithm. As the k-means clustering may stop in local minima, the algorithm was restarted 50 times, and the solution minimizing the intra-cluster distance was selected. After the extraction of these maps, we performed another clustering step on the found single-subject topographies, to obtain grand-average centroids. We imposed that for each topography set, the topography could be assigned to only one of the grand-average maps. The grand-average topographies were sorted by visual similarity to the canonical set of microstates previously reported (Michel and Koenig, 2018). Finally, each single-subject topography was matched with the grand-average one that minimized the global map dissimilarity of the pair. Group-level maps were also computed as the centroids of the maps belonging to each group of subjects.

Grand-average topographies were subsequently fitted back into the EEG signals of single subjects, with a winner-takes-all procedure: the microstate minimizing the GMD with the map of a given timepoint was assigned to that timepoint. The back-fitting was smoothed to avoid having small segments of microstate activations. Specifically, we rejected segments with duration <30 ms, by iteratively assigning the microstate label to the second best if the time duration of the segment was <30 ms (Poulsen et al., 2018).

The microstate extraction was performed using the EEGLAB Microstate plugin[2], while the back-fitting with the Microstate EEGLAB toolbox (Poulsen et al., 2018).

2.6. Microstate features extraction

For each subject, we both performed an analysis of microstate topographies and extracted a set of features characterizing the dynamics of the microstate sequence. As regards topographical differences, we assessed whether group-level topographies were statistically different between groups. First, we applied multi-group TANOVA (Koenig and Melie-García, 2009) to assess with a non-parametric permutation test differences in the global topographies. Multi-group TANOVA compares a generalized measure of difference between group maps and the grand-averages with the generalized measure of difference of a surrogate null

[2] https://www.thomaskoenig.ch/index.php/software/microstates-in-eeglab.

distribution generated by randomly shuffling the label of single-subjects maps n times (we chose n = 10000). For each similarity-matched set of microstates, we compared them using multi-group TANOVA. After assessing differences in the three groups, pairwise post-hoc comparison were performed using the TANOVA test (Murray et al., 2008). The TANOVA test works in the same way as the multi-group version, but simply compares pairwise GMD of the given maps.

Furthermore, on the subset of patients having CSF biomarkers, to explore the relation between CSF biomarkers and microstate topographies, we computed the TANOVA dissimilarity based on ATN classification (Ebenau et al., 2020). Specifically, we compared A + with A- patients, as well as subjects having at least two positive factors (one of them being A+, defined as confirmed Alzheimer's pathology) with those that had not the confirmed Alzheimer's pathology.

From the back-fitted microstate signals, we obtained a discrete sequence by only considering transition between states and we computed several descriptors for each subject. Specifically, we extracted each microstate's coverage, namely the percentage of time a given microstate remains active over the total time. We also computed the occurrence per second of each microstate. From the transition sequence, that is the sequence of transitions from a microstate to the other, we computed transition probabilities. Transition probabilities t_{ij} were defined as the probability of passing to microstate j, given the current state is microstate i. We then computed the non-linear complexity of the transitioning sequence by means of the Lempel-Ziv compression algorithm. Lempel-Ziv complexity is an index of the richness of a sequence with a finite number of generating elements (in our case, microstate labels). It measures the number of "sub-words" that can be found in the entire sequence. The higher the Lempel-Ziv complexity, the more complex is the signal. We computed this measure of complexity by measuring the length of the encoding dictionary of the sequence, by means of the *zlib* Python package (after removal of the Huffman coding component) and we normalized it by the total length of the signal to account for sequence length's differences. Finally, we computed the Hurst exponent of the microstate sequence, as described for EEG microstates (Van de Ville et al., 2010), using the implementation in the +microstate toolbox (Tait and Zhang, 2022). The Hurst exponent describes the long-term memory of the sequence, with a value of 0.5 indicating a random-walk sequence, and value of 1 indicating a totally correlated sequence.

2.7. Statistical tests

For each domain of variables (spectral, network, microstates) taken into account, normality was assessed by Shapiro-Wilk test. When the domain displayed normal behavior in most variables, we used one-way ANOVA to compare the three groups, followed by *t*-test post-hoc tests for pairwise comparisons. Otherwise, we used the non-parametric Kruskal-Wallis test to compare the three groups, followed by Wilcoxon rank sum post-hoc tests to compare medians pairwise. All post-hoc comparisons were corrected with the Bonferroni method. We used η^2 as a measure of the effect size of either ANOVA or Kruskal-Wallis tests, and Cohen's d as a measure of the effect size of the pairwise comparisons.

All analysis were performed with custom scripts in Matlab 2020b, using the EEGLAB toolbox and other plugins where specified.

3. Results

3.1. PSD and network metrics

First, we addressed the spectral differences among groups. Overall, the three conditions displayed differences in the delta band relative power and, to a lesser extent, in the alpha peak relative power, with MCI displaying the strongest delta and the weakest alpha (Fig. 2A).

Statistically, the differences were significant for the delta band (ANOVA F-statistic = 3.29, p = 0.041, $\eta^2 = 0.052$), but not in the alpha band (ANOVA F-statistic = 2.24, p = 0.111, $\eta^2 = 0.036$). Post-hoc testing between group pairs in the delta band did not reveal any significant difference at the average power level (*t*-test post-hoc, HC vs. SCD: p = 0.707, Cohen's d = 0.25, HC vs. MCI: p = 0.063, Cohen's d = 0.64, SCD vs. MCI: p = 0.163, Cohen's d = 0.385). We then repeated the comparison dividing the scalp into six ROIs (see Methods section 2.3 for

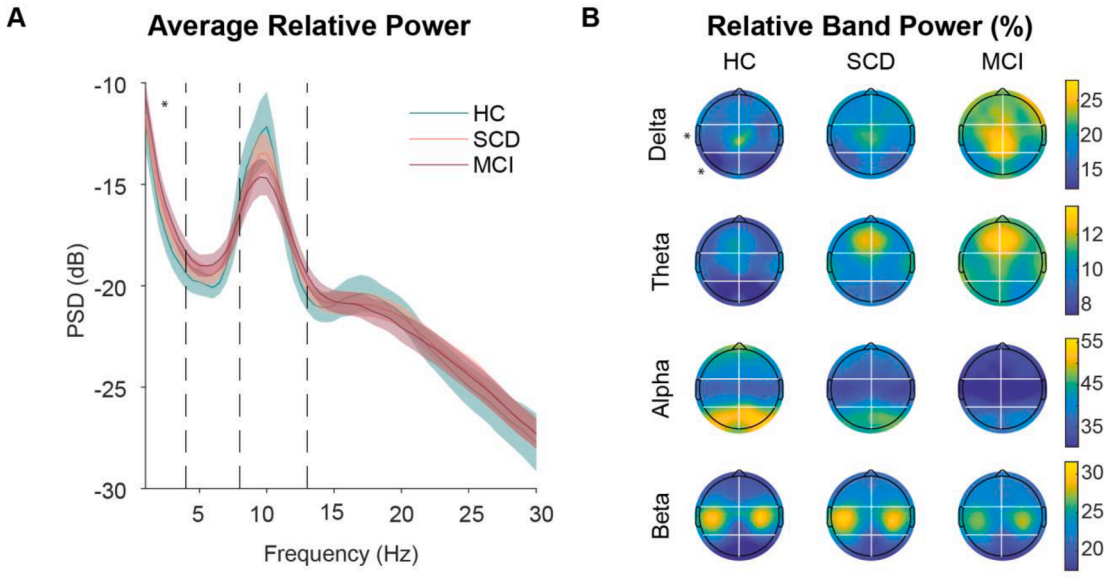

Fig. 2. Power Spectral Density (PSD) analysis. (A) Mean relative power over SCD (red curve) and MCI (blue curve) groups, averaged across all EEG channels. The value of PSD is expressed in decibel in the frequency range 1–30 Hz. Solid lines represent mean value, while shaded areas show the 95% confidence interval of the PSD distribution. (B) Topographies of power distributions in the two conditions in four frequency bands: delta (1–4 Hz, upper left), theta (4–8 Hz, upper right), alpha (8–13 Hz, lower left), beta (13–30 Hz, lower right). Topographies are shown by using the 10/20 standard coordinates on the MNI template. Black lines within the topography represent the edges of the defined ROIs. Power is expressed as the percentage of band power compared to the total power in the range 1–48 Hz. Colorbar lower and upper bounds are set to the 5th and 95th percentile of the power distribution respectively. In all panels, the significance of the corresponding statistical test (see Methods) is represented as follow: * $p < 0.05$, ** $p < 0.01$, *** $p < 0.001$. (For interpretation of the references to colour in this figure legend, the reader is referred to the web version of this article.)

details). Again, highest effects were found in delta and alpha bands. In the delta band, the left central and occipital ROIs displayed significant differences among groups but small effect size (central: ANOVA F-statistic = 3.47, p = 0.034, η^2 = 0.055; occipital: ANOVA F-statistic = 3.30, p = 0.040, η^2 = 0.052) (Fig. 2B). Post-hoc comparisons in these two areas revealed a significant increase in the delta power in the left central ROI in the MCI group, when compared to HC (*t*-test post-hoc: p = 0.047, Cohen's d = 0.645). No significant differences were found in the other bands in any ROI.

The analysis of the absolute spectral power yielded similar but non-significant results: the delta band displayed smaller differences, while the highest effects were found in the alpha band. However, no statistical difference was found at the average channel level (ANOVA, delta: F = 0.165, p = 0.848, η^2 = 0.003, theta: F = 0.61, p = 0.544, η^2 = 0.010, alpha: F = 2.51, p = 0.086, η^2 = 0.041, beta: F = 2.12, p = 0.125, η^2 = 0.034), nor at the ROI level.

We conclude that, although spectral alterations might be induced by the MCI condition, their reliability is too low to lay the ground for EEG-based early prediction of dementia.

Since the only significant difference was found in the delta range, we focused to investigate network modifications first in this specific band. Specifically, among the computed network metrics (average node strength (Fig. 3A), weighted clustering coefficient (Fig. 3B), weighted path length (Fig. 3C) and small-world index (Fig. 3D)), the only one with significant changes among groups was the small-worldness (Fig. 3D) (Kruskal-Wallis H-statistic = 9.548, p = 0.0085). Interestingly, SCD small-worldness resulted significantly higher compared to MCI (Wilcoxon post-hoc: p = 0.012, Cohen's d = 0.56) but not to HC (Wilcoxon post-hoc: p = 0.119, Cohen's d = 0.63). The small-worldness metric did not display significant differences in the other bands (theta: Kruskal-Wallis H-statistic = 4.137, p = 0.126, alpha: Kruskal-Wallis H-statistic = 4.322, p = 0.115, beta: Kruskal-Wallis H-statistic = 2.776, p = 0.250), nor did the others network metrics (p > 0.05 for all tests).

3.2. Microstate analysis

To investigate changes in the overall topographical maps of activity in the different conditions, we then decomposed the scalp EEG according to standard microstates (Michel and Koenig, 2018) (see section 2.5 for details). The shape of the microstates was not different across the three conditions (multi-group TANOVA average dissimilarity: microstate A d = 0.316, p = 0.79; microstate B d = 0.583, p = 0.32; microstate C d = 0.353, p = 0.71; microstate D d = 0.459, p = 0.40). By back-fitting grand-average maps (Fig. 4A) into single-subject data, the temporal activity of scalp EEG was decomposed into a discrete sequence of microstates (Fig. 4B).

We compared duration (Fig. 4C), coverage and occurrence (Fig. 4D) of each microstate among groups. We found significant differences in both the duration and coverage of microstate C (duration: Kruskal-Wallis H-statistic = 10.747, p = 0.0046; coverage: Kruskal-Wallis H-statistic = 7.837, p = 0.0199).

Post-hoc testing revealed that microstate C displayed a decreased duration and coverage in MCI compared to HC (Wilcoxon post-hoc, duration: p = 0.029, Cohen's d = 0. 65, coverage: p = 0.080, Cohen's d = 0.73) and SCD (Wilcoxon post-hoc, duration: p = 0.032, Cohen's d = 0.42; coverage: p = 0.075, Cohen's d = 0.50). Microstate B displayed a change in both coverage and occurrence rate (coverage: Kruskal-Wallis H-statistic = 6.25, p = 0.044; occurrence: Kruskal-Wallis H-statistic = 6.84, p = 0.0326). In this case, an increase in both coverage and frequency of occurrence was found in MCI, compared to SCD only (Wilcoxon post-hoc, coverage: p = 0.0385, Cohen's d = 0.54, occurrence: p = 0.0443, Cohen's d = 0.52). Finally, a significant variation in microstate A coverage appeared (Kruskal-Wallis H-statistic = 7.65, p = 0.022), with an increase in the SCD group compared to HC (Wilcoxon post-hoc, p = 0.0178, Cohen's d = 0.81).

Further significant differences were found in transition probabilities among microstates (Fig. 4E, see Results for the complete statistics), coherently with changes in duration of each state. Even more interestingly, the structure of the temporal patterns of microstates was significantly altered in MCI, as indicated by a decrease in the LZ complexity compared to SCD (see section 2.6, Fig. 4F, left): Kruskal-Wallis H-statistic = 9.02, p = 0.011, post-hoc SCD vs MCI: p = 0.026, Cohen's d = 0.45). Moreover, the long-term memory measured through the Hurst exponent (see section 2.6 for details) resulted in microstate patterns closer to a random walk, both in SCD and MCI compared to HC (Kruskal-Wallis H-statistic = 11.05, p = 0.0040, post-hoc HC vs SCD: p = 0.018, Cohen's d = 0.63; SCD vs MCI: p = 0.002 8, Cohen's d = 0.87; Fig. 3**F**, right). These results show that the temporal structure of microstates is reliably altered in MCI.

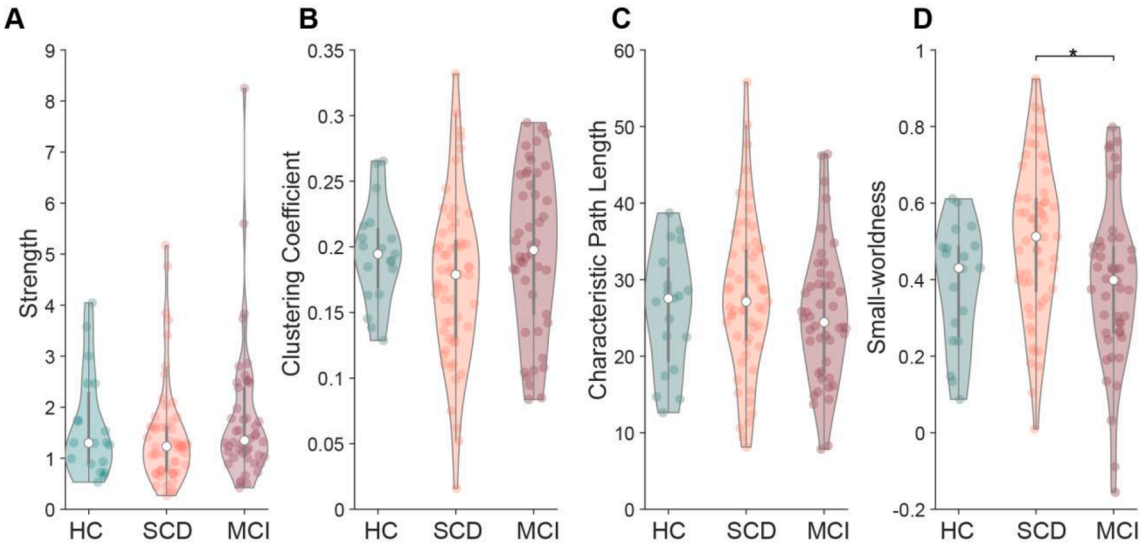

Fig. 3. Network metrics. (A) Average node strength. (B) Weighted clustering coefficient. (C) Weighted characteristic path length. (D) Small-world index (Ω). In all panels, the significance of the corresponding statistical test (see Methods) is represented as follow: * p < 0.05, ** p < 0.01, *** p < 0.001. In violin plots the inner thick line represents the interquartile range of the distribution; the thin line shows the lower/upper adjacent values (1st quartile −1.5 IQR and 3rd quartile + 1.5 IQR respectively). Shaded area represents the distribution of the data, as computed by kernel density estimate, and each datapoint is represented inside as a dot.

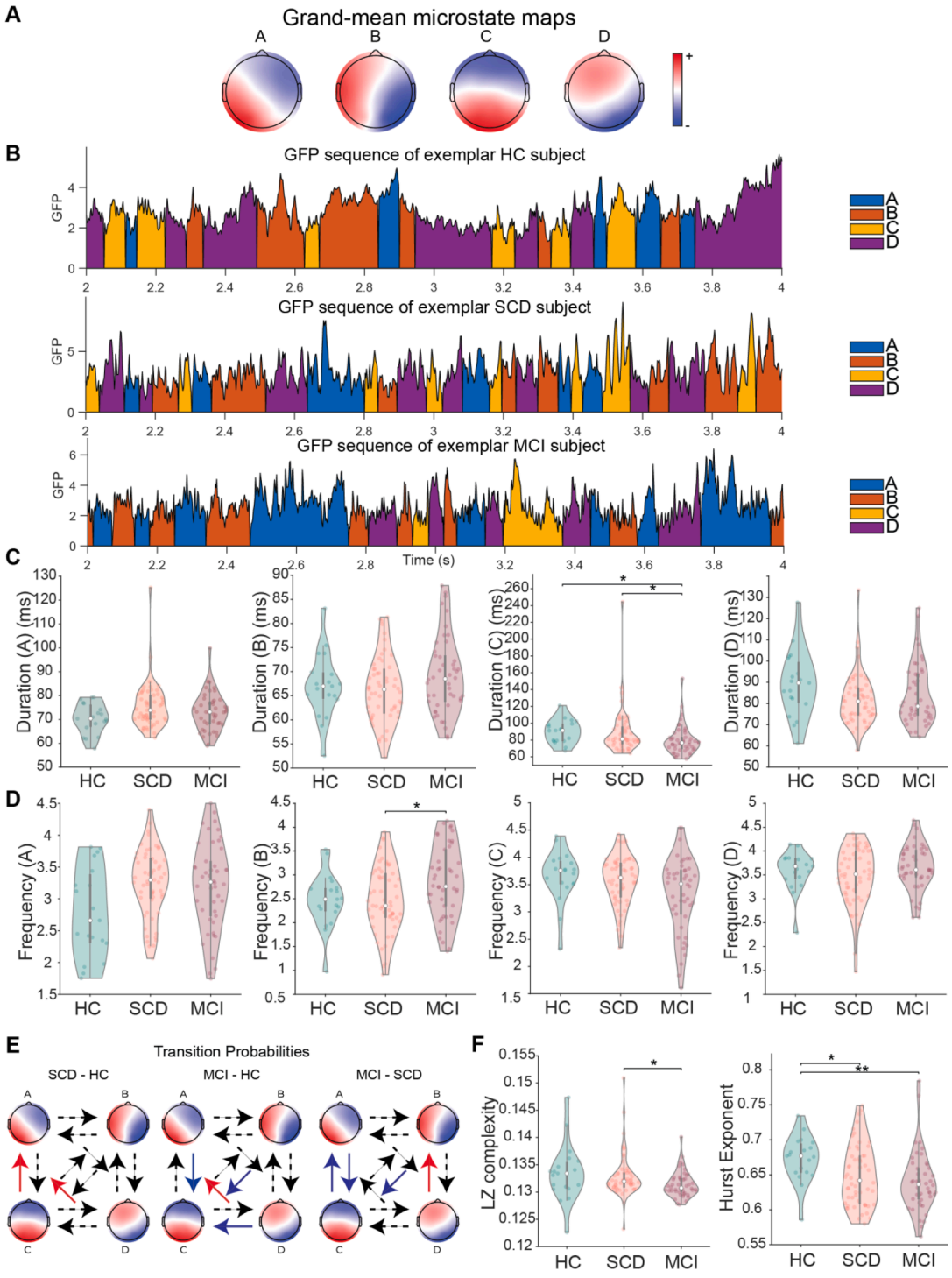

Fig. 4. Microstate metrics. (A) Grand-average microstate maps obtained by clustering single-subject topographies. (B) Example global field power (GFP) time courses for one HC (upper), one SCD subject (middle) and one MCI subjects (lower), in 2 s of continuous EEG signal. The GFP course is colored based on the active microstate in that time-point (Blue – Microstate A, Orange – Microstate B, Yellow – Microstate C, Purple – Microstate D). Qualitatively more prominence of the Microstate C can be observed in the MCI subject compared to the SCD one, as well as an overall less complex pattern of transitions. (C) Duration distributions in the three groups for each pair of microstates. The value is expressed as fraction of total time in which the EEG signal is covered by one microstate. (D) Frequency distribution of in the three groups for each pair of microstates, expressed as number of times the microstate appears per second. (E) Differences in transition probabilities among groups. The dashed arrow indicates that the transition from microstate at the base of the arrow is not different from the one at the tip of the arrow. A red arrow indicates a statistical increase in the pairwise comparison, while a blue arrow indicates a decrease in the transition probability (F) Lempel-Ziv complexity (left) and Hurst exponent (right) in the two groups. In all panels, the significance of the corresponding statistical test (see section 2.6) is represented as follow: * $p < 0.05$, ** $p < 0.01$, *** $p < 0.001$. In violin plots the inner thick line represents the interquartile range of the distribution; the thin line shows the lower/upper adjacent values (1st quartile −1.5 IQR and 3rd quartile + 1.5 IQR respectively). Shaded area represents the distribution of the data, as computed by kernel density estimate, and each datapoint is represented inside as a dot. (For interpretation of the references to colour in this figure legend, the reader is referred to the web version of this article.)

3.3. Microstate topographies based on ATN classification

So far, our analysis focused on the relationship between neural activity and clinical conditions (HC, SCD and MCI) defined by neuropsychological assessments (see section 2.6). However, patients can have similar behavior even if the underlying progression of dementia is at different stages. To assess the relationship between EEG markers and this latter aspect, we acquired CSF biomarkers from a subset of our SCD and MCI subjects (n = 50, SCD = 30, MCI = 20, see section 2.1). We tested if the positivity to CSF markers was also associated to detectable changes in microstates topology. No difference was present among microstates when grouping by amyloid pathology (A+ (n = 16, of which 8 SCD and 8 MCI) vs A- (n = 34, of which 22 SCD and 12 MCI), TANOVA dissimilarity: microstate A d = 0.036, p = 0.433; microstate B d = 0.031, p = 0.597; microstate C d = 0.029, p = 0.570; microstate D d = 0.004, p = 0.928, Bonferroni corrected, Fig. 5A). However, we found that the shape of the microstate C was significantly different between carriers of AD pathology (n = 10, of which 4 SCD and 6 MCI) and non-carriers (n = 40 of which 26 SCD and 14 MCI) (TANOVA dissimilarity: microstate A d = 0.032, p = 0.552; microstate B d = 0.048, p = 0.468; microstate C d = 0.124, p = 0.028; microstate D d = 0.060, p = 0.255, Bonferroni corrected, Fig. 5B).

4. Discussion

Our work concurrently analyzed EEG features as power spectra, connectivity, and microstate markers in SCD, MCI and healthy controls. We found that some of these EEG features significantly differ across conditions. In particular, microstates are the most robust marker of differentiation between subjective and objective cognitive decline. The degradation of microstate C resulted in a lesser complexity of the microstate sequence in MCI. Results were even stronger when taking into account the AD CSF biomarkers profile in a subgroup of patients, as in this case microstate C topology itself was altered. These results suggest that the possible progression from subjective to objective cognitive decline might be associated to a change in the global structure of cortical activity that can be properly detected by microstate analysis.

The increasing interest in characterizing SCD is due to the possibility of intercepting Alzheimer's Disease at the earliest stages of the pathology. SCD constitute a heterogeneous group, as it could be related to conditions such as normal aging, personality traits, psychiatric conditions, neurologic and medical disorders, substance use, and medication (Margolis et al., 2020). Therefore, understanding whether SCD is a valid concern and finding the most cost-effective tools to ascertain this is crucial both for people experiencing SCD and for targeting dementia prevention (Vellas et al., 2011). Several efforts have been put to this aim, identifying demographic (Mazzeo et al., 2020), cognitive (Bessi et al., 2018; Chary et al., 2013; Mazzeo et al., 2019b; Silva et al., 2012; Wolfsgruber et al., 2020), genetic (Ali et al., 2018; Bessi et al., 2020b, 2020a; Mazzeo et al., 2022; Mazzeo et al., 2021; Mazzeo et al., 2019a) and brain structure (Wang et al., 2020) features to stratify SCD patients according to the risk of progression to objective cognitive decline.

In the last years, the potential use of EEG for diagnosing dementia pathologies, and in particular AD has been extensively investigated (Alberdi et al., 2016; Gouw et al., 2017; Malek et al., 2017). However, previous research has mostly focused on the classification of either healthy controls and MCI (or AD dementia patients), or healthy controls and SCD subjects. In this study we focused our attention on the

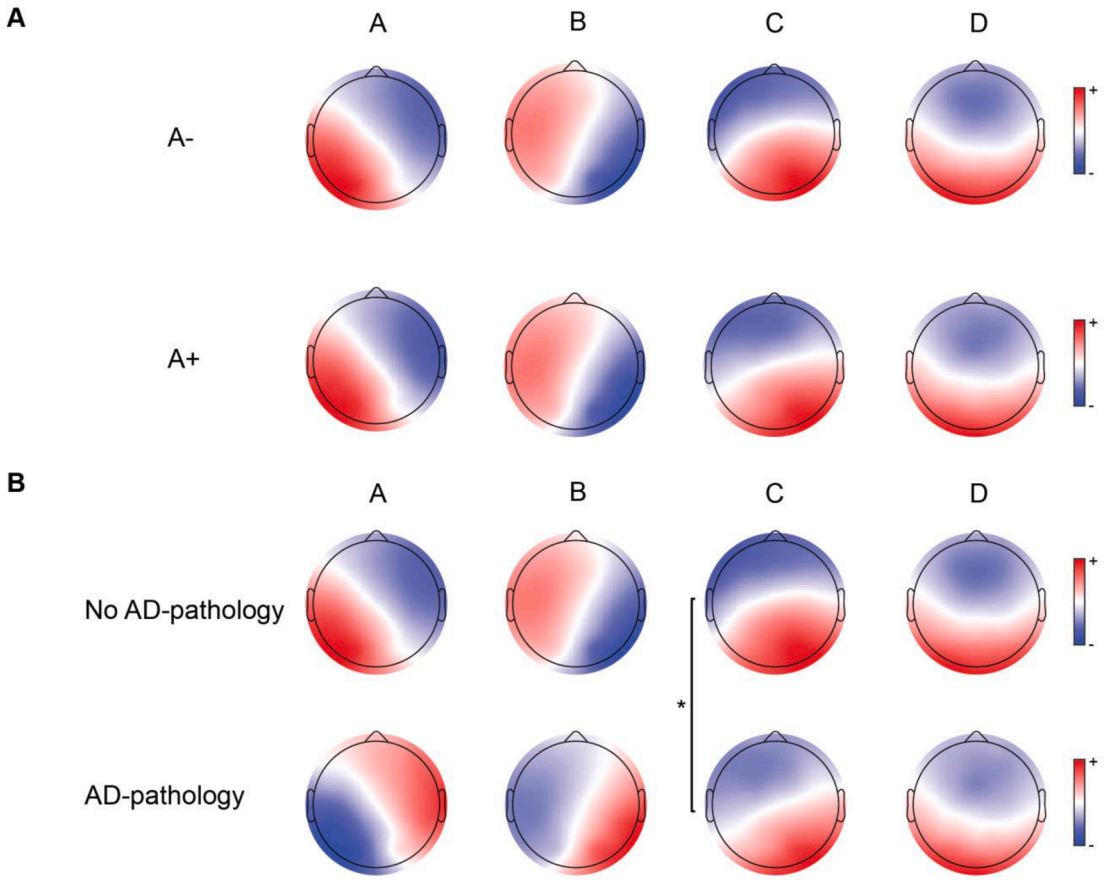

Fig. 5. Topographical differences in ATN classification. (A) Group-level mean topographies of Amyloid negative (A-) and Amyloid positive (A +) subjects. (B) Group-level mean topographies of SCD or MCI subjects due to Alzheimer's Disease (AD pathology) and not due to Alzheimer's Disease (No AD-pathology). In all panels, the significance of the corresponding statistical test (see section 2.7) is represented as follow: * $p < 0.05$, ** $p < 0.01$, *** $p < 0.001$.

discrimination between SCD and MCI conditions, as we aimed to explore possible biomarkers of the ongoing cognitive decline. Such biomarkers should be cross-sectionally present in the MCI group, while should only be present in the subset of SCD that will develop the dementia. Hence, comparing these "closer" groups should help highlighting differences related to the onset of the disease and that could possibly be used as candidate biomarkers for longitudinal studies.

4.1. Spectral analysis

Our spectral results show a degree of similarity with the findings of previous research. In a previous work (Smailovic et al., 2018) a large cohort (>600 total subjects) of memory clinic patients was tested for differences in the spectral activity of SCD, MCI and Alzheimer's patients. While the three-groups comparison highlighted differences in global field power in the delta, theta and alpha bands, these differences were mostly due to the EEG profile of Alzheimer's patients, with less variability between the SCD and MCI groups. This is in accordance with what we found for power spectra at the sensors' level (Fig. 2). In another work (Jeong et al., 2021), EEG power spectra of SCD patients were compared to healthy controls, and higher frontal-channels delta activity was found. While this is not true for the channel-level spectra in our data, we found similar trends in the delta band, although not significant. Our trends are also in line with the MEG study by López-Sanz and colleagues (López-Sanz et al., 2016) in which they claim that alpha band power decreases similarly in SCD and MCI compared to controls, but the slowing of the alpha band peak is only visible in the MCI cohort. Another work (Babiloni et al., 2010) found differences in spectral power of cortical sources in the parietal and occipital theta in SCD patients, as well as greater amplitude in the alpha band comparing SCD and MCI subjects. Differences with these results, while being partially in line with ours, may be due to the use of source power and a different subdivision in frequency bands (dividing alpha in two sub-bands).

Overall, the lack of clear spectral differences between the two groups may indicate that the whole-brain changes that underpin the slowing in the oscillations widely observed for Alzheimer's Disease are not yet markedly visible in the SCD condition. Further studies should investigate whether taking other risk factors into account (e.g. by following the SCD*plus* criteria subdivisions (Jessen et al., 2014)) may reveal subgroups of SCD or MCI patients in which the neurodegeneration is more apparent at the spectral level.

However, spectral differences may be obscured by the inherent inter-subject variability of power measurements in the EEG signal (e.g. due to the variability in the alpha peak (Haegens et al., 2014)). Hence, the lack of statistical significance of spectral features in our cross-sectional study does not rule out their possible importance in longitudinal studies.

4.2. Network metrics

On the other side, recent evidence suggests that connectivity-based approaches may be more able to characterize SCD with respect to other pathological stages of dementia (Lazarou et al., 2019). For frequency-based connectivity estimates, a decrease in the degree of connections has been reported in AD and MCI (Babiloni et al., 2018a, 2006; Rossini et al., 2006). We did not find any difference among groups in the average strengths of the connection between brain areas. To avoid widely increasing the number of possible comparisons, we focused on the average strength over all brain areas, a measure that may not be sensitive enough to capture subtle differences in connectivity that may appear early in the cognitive decline process. This may be the reason why we did not find decreased connectivity even in the MCI cohort when compared to HC, as previously reported in other studies. Focusing on area-specific connections, we may find differences appearing even early in the AD continuum.

Moreover, the small-worldness metric was reported to be disrupted in Alzheimer's Disease (Vecchio et al., 2018). Interestingly, we found alterations of the small-world metric in the delta band in the SCD cohort, even though these changes normalize in the MCI group (see Fig. 3D). This u-shaped difference deserves further investigation but might be sub-optimal for decoding the patient's clinical condition. Undergoing computational studies suggest that the increase in small-worldness only present in SCD patients is due to some form of protection mechanisms against the onset of the decline. In any case the differences with other studies (e.g. (Frantzidis et al., 2014; Xu et al., 2020)) may be due to several reasons: first, connectivity-based estimates of network properties are greatly influenced by methodological choices, especially related to source localization and the adopted connectivity metric, as reported (Mahjoory et al., 2017). Secondly, small-worldness is a summary metric that is computed at the whole-brain level. In the case of the conditions we are analyzing, global changes in the network properties of the system may not be observable at the stage of SCD or MCI, especially using time-invariant connectivity estimates. In this sense, using a simpler clustering approach that can still capture connectivity patterns in the data, even modelling dynamic transitions, such as microstate analysis, revealed better in increasing the discriminating capability.

4.3. Microstate analysis

Microstate analysis was already used in the past to discriminate between SCD, MCI and AD by (Smailovic et al., 2019). In their work, several differences have been highlighted in microstates characteristics comparing HC, SCD and MCI groups. Specifically, they identified altered topographies of the microstate A and D in each clinical condition compared to controls, and differences between SCD and controls for the microstate C. Conversely, we did not identify any topographical difference based on cognitive characterization (HC, SCD, MCI). Despite the consistent differences in this result, we hypothesize it may be due to the much larger number of participants in the study of Smailovic and colleagues compared to ours: the increased power of their sample allowed them to detect smaller differences in map topographies. These topographical differences prevent direct comparison with our results regarding duration, coverage, and occurrence.

One key advancement relative to the work of Smailovic are our analysis of the temporal patterns of the microstates. First, we found significant differences in transition probabilities. Then, we also applied for the first time on an SCD cohort the computation of LZ complexity of the microstate sequence (Tait et al., 2020). The complexity of signals disruption, widely observed in the case of Alzheimer's in EEG and MEG (e.g. (Tait et al. 2020; Shumbayawonda et al., 2020)) may also hold true in characterizing the difference between SCD and MCI. LZ complexity has been selected over other metrics of complexity of EEG signals, such as Approximate and Sample entropy (Delgado-Bonal and Marshak, 2019) as it is optimized to handle discrete sequences of symbols, such as the microstate sequence. LZ complexity is known to be a robust marker of brain dysfunction, both when computed at the signal level (e.g. in depression (Bachmann et al., 2015), schizophrenia (Ibáñez-Molina et al., 2018) and epilepsy (Abásolo et al., 2007; Bai et al., 2015)) and at microstates level (for example (Artoni et al., 2022; Tait et al., 2020; Zhao et al., 2022)).

LZ complexity measures the diversity of patterns in the signal (in this case, the microstates sequence). It is a proxy measure for the loss of the information conveyed by the temporal evolution of cortical activity as this might occur since the earliest stages of cognitive decline. Indeed, our results show that the progression of cognitive decline is associated with a reduction in LZ complexity.

We also introduced for the first time the Hurst exponent in the analysis of the microstate sequence in the SCD cohort: it revealed a gradient-like pattern of the long-term memory of the microstate sequence towards the random walk behavior as the cognitive decline progresses. Since the Hurst exponent in healthy adults correlates with long-term dependencies in the microstate sequence (Van de Ville et al., 2010), our results suggest that a loss of long-term temporal connections

in the EEG signal may be a hallmark of cognitive decline.

Moreover, such alterations to EEG microstates in the path towards dementia may not only be a tool to early diagnose the disease, but also a first step towards the development of therapies to at least alleviate the symptoms of AD. Recently, gamma audiovisual flicker stimulation has been proven a valid tool to reduce the symptoms of AD (Iaccarino et al., 2016), even in humans with prodromal phases of the disease (He et al., 2021). In a recent work (Zhang et al., 2021) it has been shown that gamma entrainment alters microstate dynamics (coverage, transition probabilities and Lempel-Ziv complexity) in healthy subjects compared to control stimulation.

EEG microstates have also been extensively applied to the study of other neurological disorders, especially schizophrenia. Several schizophrenia studies report an increase in the occurrence of microstate C compared to controls (Kikuchi et al., 2011; Nishida et al., 2013). In depression, studies have often reported variation of the microstate D temporal patterns (Li et al., 2021; Murphy et al., 2020). At the same time, the microstate C duration is reduced compared to controls also in other forms of dementia, such as frontotemporal dementia (Nishida et al., 2013). When comparing SCD and MCI, we observe instead a trend toward a decrease of microstate C occurrence and duration from SCD to MCI, and no differences in microstate D properties. This suggests there may be divergent pathways between neurodegenerative and psychiatric diseases.

4.4. Microstate topographies based on ATN classification

Smailovic and colleagues (Smailovic et al., 2019) showed that changes in the topography of microstate class C were associated with the CSF $A\beta_{42}$ levels. Differently, we found no significant difference between the A + and A− cohorts. However, we found significant differences in the microstate C topography when comparing the AD-like CSF profile group (A + associated with T + and/or N +) with the non-AD CSF profile. This may be due to our further categorization based on two CSF markers, able to reveal more subtle differences in the topographies of the groups compared to the single-marker classification.

Moreover, we hypothesize that the differences that we found in the microstate temporal sequence in the cognitive characterization of the subjects (SCD and MCI), mostly found in microstate C, convert to topographical changes when selecting the subset of patients with AD pathology. In this view we could hypothesize that differences in the microstate C topography could be predictive of a future progression to dementia, being present in the subgroup of individuals more at risk for progression to AD dementia. Naturally, the evolution of individuals over time will serve to confirm these data.

Interestingly, microstate C topography has been previously related to object-visual thinking (Milz et al., 2016) and to attention reorientation (Britz et al., 2010), hence highlighting how these two features may get disrupted early on in the cognitive decline process.

4.5. Limitations

Our study presents some limitations that should be addressed in future works. First, the sample size of our work is relatively limited if compared to some of the previous works (Smailovic et al., 2019; Smailovic et al., 2018). In particular, the limited number of subjects with CSF did not allow for a complete two-factors study of the interplay between the clinical and ATN classification in determining EEG microstates. Another limitation is the lack of patients with full Alzheimer's dementia, that could have helped in better checking whether the identified features are coherently describing the decline in all its stages.

Another limitation of the current work is the absence of age matching between the SCD and MCI groups. While this is an inherent property of the cohort, due to the later occurrence of MCI in the Alzheimer's continuum (Bessi et al., 2018; Smailovic et al., 2019), the different ages of the two groups may enhance some of the effects found in the identified markers (Rempe et al., 2023; Zappasodi et al., 2015). However, the differences found between SCD and MCI in microstate C duration and occurrence have an opposite sign compared to the age-related differences in the available literature (Koenig et al., 2002), corroborating our conclusions.

An additional limitation in our results may be due to the limited amount of control subjects that were recruited. However, most of the results are robust to the unbalance in the sample sizes of the three groups thanks to the use of non-parametric tests.

Finally, we also need to take into account that the SCD cohort is by definition a heterogeneous group, in which people that will develop a form of dementia coexist with healthy elderly. Since our sample size was limited, we only considered a limited number of possible covariates, most notably the CSF biomarkers. However, it will be necessary in future studies to investigate the relationship between EEG features and other neuropsychological characteristics, in order to better cluster subjects within the SCD condition.

4.6. Perspectives and future studies

This work demonstrated the possibility of finding resting-state EEG markers between two stages of cognitive decline cross-sectionally, by comparing different analysis methods. To the best of our knowledge, this is the first study assessing possible spectral, connectivity and microstate markers simultaneously in the same cohort of SCD and MCI subjects. Additionally, we introduced some features, such as the Hurst exponent, that were not previously used to describe the pre-clinical stages of AD but displayed significant differences across conditions.

In conclusion, microstate analysis revealed to be the most prominent EEG marker to distinguish SCD, MCI and controls. Several improvements to this study will be explored in the future as the study PREVIEW goes on. First, current SCD patients will be followed-up to track changes in their EEG metrics behavior and ultimately to check whether it is possible to prognostically use the methods we developed here to predict the onset of MCI or Alzheimer's Dementia. Finally, a cross-validated machine learning algorithm will be developed to assess the prediction capability of the found markers to distinguish longitudinally the different forms of dementia.

Funding

This project was funded by Tuscany Region - PRedicting the EVolution of SubjectIvE Cognitive Decline to Alzheimer's Disease With machine learning - PREVIEW - CUP. D18D20001300002.

The work was also supported by #NEXTGENERATIONEU (NGEU) and funded by the Ministry of University and Research (MUR), National Recovery and Resilience Plan(NRRP), project MNESYS (PE0000006) – A Multiscale integrated approach to the study of the nervous system in health and disease (DN. 1553 11.10.2022).

CRediT authorship contribution statement

Michael Lassi: Methodology, Formal analysis, Writing – original draft, Writing – review & editing, Visualization. **Carlo Fabbiani:** Investigation, Writing – original draft, Writing – review & editing. **Salvatore Mazzeo:** Methodology, Formal analysis, Investigation, Writing – original draft, Writing – review & editing. **Rachele Burali:** Investigation, Writing – review & editing. **Alberto Arturo Vergani:** Methodology, Formal analysis, Writing – review & editing. **Giulia Giacomucci:** Investigation, Writing – review & editing. **Valentina Moschini:** Investigation, Writing – review & editing. **Carmen Morinelli:** Investigation, Writing – review & editing. **Filippo Emiliani:** Investigation, Writing – review & editing. **Maenia Scarpino:** Investigation, Writing – review & editing. **Silvia Bagnoli:** Investigation, Writing – review & editing. **Assunta Ingannato:** Investigation, Writing – review & editing. **Benedetta Nacmias:** Investigation, Writing – review & editing. **Sonia**

Padiglioni: Investigation, Writing – review & editing. **Silvestro Micera:** Methodology, Formal analysis, Writing – review & editing, Supervision, Project administration, Funding acquisition. **Sandro Sorbi:** Conceptualization, Writing – review & editing, Supervision, Project administration, Funding acquisition. **Antonello Grippo:** Conceptualization, Investigation, Writing – original draft, Writing – review & editing, Supervision, Project administration, Funding acquisition. **Valentina Bessi:** Conceptualization, Investigation, Writing – original draft, Writing – review & editing, Supervision, Project administration, Funding acquisition. **Alberto Mazzoni:** Conceptualization, Methodology, Formal analysis, Writing – original draft, Writing – review & editing, Supervision, Project administration, Funding acquisition.

Declaration of Competing Interest

The authors declare that they have no known competing financial interests or personal relationships that could have appeared to influence the work reported in this paper.

Data availability

Due to the sensitivity of personal information in this research, data is available upon formal request at the local ethics committee. The code generating the results of the current study can be found at https://github.com/mikelassi/PREVIEW.

References

Abásolo, D., James, C.J., Hornero, R., 2007. Non-linear Analysis of Intracranial Electroencephalogram Recordings with Approximate Entropy and Lempel-Ziv Complexity for Epileptic Seizure Detection. Medicine and Biology Society 1953–1956. https://doi.org/10.1109/IEMBS.2007.4352700.

Alberdi, A., Aztiria, A., Basarab, A., 2016. On the early diagnosis of Alzheimer's Disease from multimodal signals: a survey. Artif. Intell. Med. 71, 1–29. https://doi.org/10.1016/j.artmed.2016.06.003.

Albert, M.S., DeKosky, S.T., Dickson, D., Dubois, B., Feldman, H.H., Fox, N.C., Gamst, A., Holtzman, D.M., Jagust, W.J., Petersen, R.C., Snyder, P.J., Carrillo, M.C., Thies, B., Phelps, C.H., 2011. The diagnosis of mild cognitive impairment due to Alzheimer's disease: recommendations from the National Institute on Aging-Alzheimer's Association workgroups on diagnostic guidelines for Alzheimer's disease. Alzheimers Dement. 7, 270–279. https://doi.org/10.1016/j.jalz.2011.03.008.

Alcolea, D., Pegueroles, J., Muñoz, L., Camacho, V., López-Mora, D., Fernández-León, A., Bastard, N.L., Huyck, E., Nadal, A., Olmedo, V., Sampedro, F., Montal, V., Vilaplana, E., Clarimón, J., Blesa, R., Fortea, J., Lleó, A., 2019. Agreement of amyloid PET and CSF biomarkers for Alzheimer's disease on Lumipulse. Ann. Clin. Transl. Neurol. 6, 1815–1824. https://doi.org/10.1002/acn3.50873.

Alexander, D.M., Arns, M.W., Paul, R.H., Rowe, D.L., Cooper, N., Esser, A.H., Fallahpour, K., Stephan, B.C.M., Heesen, E., Breteler, R., Williams, L.M., Gordon, E., 2006. Eeg markers for cognitive decline in elderly subjects with subjective memory complaints. J. Integr. Neurosci. 05, 49–74. https://doi.org/10.1142/S0219635206001021.

Ali, J.I., Smart, C.M., Gawryluk, J.R., 2018. Subjective Cognitive Decline and APOE ε4: A Systematic Review. J. Alzheimers Dis. 65, 303–320. https://doi.org/10.3233/JAD-180248.

Babiloni, C., Ferri, R., Binetti, G., Cassarino, A., Forno, G.D., Ercolani, M., Ferreri, F., Frisoni, G.B., Lanuzza, B., Miniussi, C., Nobili, F., Rodriguez, G., Rundo, F., Stam, C. J., Musha, T., Vecchio, F., Rossini, P.M., 2006. Fronto-parietal coupling of brain rhythms in mild cognitive impairment: a multicentric EEG study. Brain Res. Bull. 69, 63–73. https://doi.org/10.1016/j.brainresbull.2005.10.013.

Babiloni, C., Visser, P.J., Frisoni, G., De Deyn, P.P., Bresciani, L., Jelic, V., Nagels, G., Rodriguez, G., Rossini, P.M., Vecchio, F., Colombo, D., Verhey, F., Wahlund, L.-O., Nobili, F., 2010. Cortical sources of resting EEG rhythms in mild cognitive impairment and subjective memory complaint. Neurobiol. Aging 31, 1787–1798.

Babiloni, C., Del Percio, C., Lizio, R., Noce, G., Lopez, S., Soricelli, A., Ferri, R., Nobili, F., Arnaldi, D., Famà, F., Aarsland, D., Orzi, F., Buttinelli, C., Giubilei, F., Onofrj, M., Stocchi, F., Stirpe, P., Fuhr, P., Gschwandtner, U., Ransmayr, G., Garn, H., Fraioli, L., Pievani, M., Frisoni, G.B., D'Antonio, F., De Lena, C., Güntekin, B., Hanoğlu, L., Başar, E., Yener, G., Emek-Savaş, D.D., Triggiani, A.I., Franciotti, R., Taylor, J.P., Vacca, L., De Pandis, M.F., Bonanni, L., 2018a. Abnormalities of resting-state functional cortical connectivity in patients with dementia due to Alzheimer's and Lewy body diseases: an EEG study. Neurobiol. Aging 65, 18–40. https://doi.org/10.1016/j.neurobiolaging.2017.12.023.

Babiloni, C., Del Percio, C., Lizio, R., Noce, G., Lopez, S., Soricelli, A., Ferri, R., Pascarelli, M.T., Catania, V., Nobili, F., Arnaldi, D., Famà, F., Orzi, F., Buttinelli, C., Giubilei, F., Bonanni, L., Franciotti, R., Onofrj, M., Stirpe, P., Fuhr, P., Gschwandtner, U., Ransmayr, G., Garn, H., Fraioli, L., Pievani, M., D'Antonio, F., De Lena, C., Güntekin, B., Hanoğlu, L., Başar, E., Yener, G., Emek-Savaş, D.D., Triggiani, A.I., Taylor, J.P., De Pandis, M.F., Vacca, L., Frisoni, G.B., Stocchi, F., 2018b. Functional cortical source connectivity of resting state electroencephalographic alpha rhythms shows similar abnormalities in patients with mild cognitive impairment due to Alzheimer's and Parkinson's diseases. Clin. Neurophysiol. 129, 766–782. https://doi.org/10.1016/j.clinph.2018.01.009.

Artoni, F., Maillard, J., Britz, J., Seeber, M., Lysakowski, C., Bréchet, L., Tramèr, M.R., Michel, C.M., 2022. EEG microstate dynamics indicate a U-shaped path to propofol-induced loss of consciousness. NeuroImage 256, 119156. https://doi.org/10.1016/j.neuroimage.2022.119156.

Babiloni, C., Barry, R.J., Başar, E., Blinowska, K.J., Cichocki, A., Drinkenburg, W.H.I.M., Klimesch, W., Knight, R.T., Lopes da Silva, F., Nunez, P., Oostenveld, R., Jeong, J., Pascual-Marqui, R., Valdes-Sosa, P., Hallett, M., 2020. International Federation of Clinical Neurophysiology (IFCN) – EEG research workgroup: Recommendations on frequency and topographic analysis of resting state EEG rhythms. Part 1: Applications in clinical research studies. Clin. Neurophysiol. 131, 285–307. https://doi.org/10.1016/j.clinph.2019.06.234.

Bachmann, M., Kalev, K., Suhhova, A., Lass, J., Hinrikus, H., 2015. Lempel Ziv Complexity of EEG in Depression. Springer International Publishing, Cham, pp. 58–61. https://doi.org/10.1007/978-3-319-11128-5_15.

Bai, Y., Liang, Z., Li, X., 2015. A permutation Lempel-Ziv complexity measure for EEG analysis. Biomedical Signal Processing and Control 19, 102–114. https://doi.org/10.1016/j.bspc.2015.04.002.

Bastos, A.M., Schoffelen, J.-M., 2016. A Tutorial Review of Functional Connectivity Analysis Methods and Their Interpretational Pitfalls. Frontiers in Systems Neuroscience 9.

Bell, A.J., Sejnowski, T.J., 1995. An information-maximization approach to blind separation and blind deconvolution. Neural Comput. 7, 1129–1159. https://doi.org/10.1162/neco.1995.7.6.1129.

Bessi, V., Mazzeo, S., Padiglioni, S., Piccini, C., Nacmias, B., Sorbi, S., Bracco, L., 2018. From Subjective Cognitive Decline to Alzheimer's Disease: The Predictive Role of Neuropsychological Assessment, Personality Traits, and Cognitive Reserve. A 7-Year Follow-Up Study. J. Alzheimer's Disease 63, 1523–1535. https://doi.org/10.3233/JAD-171180.

Bessi, V., Giacomucci, G., Mazzeo, S., Bagnoli, S., Padiglioni, S., Balestrini, J., Tomaiuolo, G., Piaceri, I., Carraro, M., Bracco, L., Sorbi, S., Nacmias, B., 2020a. PER2 C111G polymorphism, cognitive reserve and cognition in subjective cognitive decline and mild cognitive impairment. A 10-year follow-up study. Eur. J. Neurol. https://doi.org/10.1111/ene.14518.

Bessi, V., Mazzeo, S., Bagnoli, S., Padiglioni, S., Carraro, M., Piaceri, I., Bracco, L., Sorbi, S., Nacmias, B., 2020b. The implication of BDNF Val66Met polymorphism in progression from subjective cognitive decline to mild cognitive impairment and Alzheimer's disease: a 9-year follow-up study. Eur. Arch. Psychiatry Clin. Neurosci. 270, 471–482. https://doi.org/10.1007/s00406-019-01069-y.

Besthorn, C., Förstl, H., Geiger-Kabisch, C., Sattel, H., Gasser, T., Schreiter-Gasser, U., 1994. EEG coherence in Alzheimer disease. Electroencephalogr. Clin. Neurophysiol. 90, 242–245. https://doi.org/10.1016/0013-4694(94)90095-7.

Bhome, R., Berry, A.J., Huntley, J.D., Howard, R.J., 2018. Interventions for subjective cognitive decline: systematic review and meta-analysis. BMJ Open 8, e021610.

Bigdely-Shamlo, N., Mullen, T., Kothe, C., Su, K.-M., Robbins, K.A., 2015. The PREP pipeline: standardized preprocessing for large-scale EEG analysis. Front. Neuroinf. 9, 1–19.

Britz, J., Van De Ville, D., Michel, C.M., 2010. BOLD correlates of EEG topography reveal rapid resting-state network dynamics. Neuroimage 52, 1162–1170. https://doi.org/10.1016/j.neuroimage.2010.02.052.

Cassani, R., Estarellas, M., San-Martin, R., Fraga, F.J., Falk, T.H., 2018. Systematic Review on Resting-State EEG for Alzheimer's Disease Diagnosis and Progression Assessment. Dis. Markers 2018, 5174815. https://doi.org/10.1155/2018/5174815.

Chary, E., Amieva, H., Pérès, K., Orgogozo, J.-M., Dartigues, J.-F., Jacqmin-Gadda, H., 2013. Short- versus long-term prediction of dementia among subjects with low and high educational levels. Alzheimers Dement. 9, 562–571. https://doi.org/10.1016/j.jalz.2012.05.2188.

Cummings, J.L., Doody, R., Clark, C., 2007. Disease-modifying therapies for Alzheimer disease: Challenges to early intervention. Neurology 69, 1622–1634. https://doi.org/10.1212/01.wnl.0000295996.54210.69.

da Cruz, J.R., Favrod, O., Roinishvili, M., Chkonia, E., Brand, A., Mohr, C., Figueiredo, P., Herzog, M.H., 2020. EEG microstates are a candidate endophenotype for schizophrenia. Nat. Commun. 11, 1–11. https://doi.org/10.1038/s41467-020-16914-1.

Delgado-Bonal, A., Marshak, A., 2019. Approximate Entropy and Sample Entropy: A Comprehensive Tutorial. Entropy 21, 541. https://doi.org/10.3390/e21060541.

Delorme, A., Makeig, S., 2004. EEGLAB: an open source toolbox for analysis of single-trial EEG dynamics including independent component analysis. J. Neurosci. Methods 134, 9–21.

Delorme, A., Sejnowski, T., Makeig, S., 2007. Enhanced detection of artifacts in EEG data using higher-order statistics and independent component analysis. Neuroimage 34, 1443–1449. https://doi.org/10.1016/j.neuroimage.2006.11.004.

Delorme, A., Palmer, J., Onton, J., Oostenveld, R., Makeig, S., 2012. Independent EEG Sources Are Dipolar. PLoS One 7, e30135.

Dierks, T., Jelic, V., Julin, P., Maurer, K., Wahlund, L.O., Almkvist, O., Strik, W.K., Winblad, B., 1997. EEG-microstates in mild memory impairment and Alzheimer's disease: possible association with disturbed information processing. J. Neural Transmission 104, 483–495. https://doi.org/10.1007/BF01277666.

Douw, L., Nieboer, D., Stam, C.J., Tewarie, P., Hillebrand, A., 2018. Consistency of magnetoencephalographic functional connectivity and network reconstruction using a template versus native MRI for co-registration. Hum. Brain Mapp. 39, 104–119. https://doi.org/10.1002/hbm.23827.

Dubois, B., Padovani, A., Scheltens, P., Rossi, A., Dell'Agnello, G., 2016. Timely Diagnosis for Alzheimer's Disease: A Literature Review on Benefits and Challenges. J. Alzheimers Dis. 49, 617–631.

Ebenau, J.L., Timmers, T., Wesselman, L.M.P., Verberk, I.M.W., Verfaillie, S.C.J., Slot, R. E.R., van Harten, A.C., Teunissen, C.E., Barkhof, F., van den Bosch, K.A., van Leeuwenstijn, M., Tomassen, J., den Braber, A., Visser, P.J., Prins, N.D., Sikkes, S.A. M., Scheltens, P., van Berckel, B.N.M., van der Flier, W.M., 2020. ATN classification and clinical progression in subjective cognitive decline. Neurology 95, e46–e58. https://doi.org/10.1212/WNL.0000000000009724.

Zhao, Z., Niu, Y., Zhao, X., Zhu, Y., Shao, Z., Wu, X., Wang, C., Gao, X., Wang, C., Xu, Y., Zhao, J., Gao, Z., Ding, J., Yu, Y., 2022. EEG microstate in first-episode drug-naive adolescents with depression. J. Neural Eng. 19, 056016 https://doi.org/10.1088/1741-2552/ac88f6.

Engedal, K., Lage Barca, M., Høgh, P., Andersen, B.B., Dombernowsky, N.W., Naik, M., Gudmundsson, T.E., Øksengaard, A.-R., Wahlund, L.-O., Snaedal, J., 2020. The Power of EEG to Predict Conversion from Mild Cognitive Impairment and Subjective Cognitive Decline to Dementia Keywords Mild cognitive impairment · Subjective cognitive decline · Dementia · EEG. https://doi.org/10.1159/000508392.

Fanciullacci, C., Bertolucci, F., Lamola, G., Panarese, A., Artoni, F., Micera, S., Rossi, B., Chisari, C., 2017. Delta Power Is Higher and More Symmetrical in Ischemic Stroke Patients with Cortical Involvement. Front. Hum. Neurosci. 385.

Ferreira, D., Jelic, V., Cavallin, L., Oeksengaard, A.-R., Snaedal, J., Høgh, P., Andersen, B. B., Naik, M., Engedal, K., Westman, E., Wahlund, L.-O., 2016. Electroencephalography Is a Good Complement to Currently Established Dementia Biomarkers. DEM 42, 80–92. https://doi.org/10.1159/000448394.

Fonseca, L.C., Tedrus, G.M.A.S., Prandi, L.R., de Andrade, A.C.A., 2011. Quantitative electroencephalography power and coherence measurements in the diagnosis of mild and moderate Alzheimer's disease. Arq. Neuropsiquiatr. 69, 297–303. https://doi.org/10.1590/s0004-282x2011000300006.

Frantzidis, C.A., Vivas, A.B., Tsolaki, A., Klados, M.A., Tsolaki, M., Bamidis, P.D., 2014. Functional disorganization of small-world brain networks in mild Alzheimer's Disease and amnestic Mild Cognitive Impairment: an EEG study using Relative Wavelet Entropy (RWE). Front. Aging Neurosci. 6, 224. https://doi.org/10.3389/fnagi.2014.00224.

Gouw, A.A., Alsema, A.M., Tijms, B.M., Borta, A., Scheltens, P., Stam, C.J., van der Flier, W.M., 2017. EEG spectral analysis as a putative early prognostic biomarker in nondemented, amyloid positive subjects. Neurobiol. Aging 57, 133–142. https://doi.org/10.1016/j.neurobiolaging.2017.05.017.

Grieder, M., Koenig, T., Kinoshita, T., Utsunomiya, K., Wahlund, L.-O., Dierks, T., Nishida, K., 2016. Discovering EEG resting state alterations of semantic dementia. Clin. Neurophysiol. 127, 2175–2181. https://doi.org/10.1016/j.clinph.2016.01.025.

Haegens, S., Cousijn, H., Wallis, G., Harrison, P.J., Nobre, A.C., 2014. Inter- and intra-individual variability in alpha peak frequency. Neuroimage 92, 46–55. https://doi.org/10.1016/j.neuroimage.2014.01.049.

He, Q., Colon-Motas, K.M., Pybus, A.F., Piendel, L., Seppa, J.K., Walker, M.L., Manzanares, C.M., Qiu, D., Miocinovic, S., Wood, L.B., Levey, A.I., Lah, J.J., Singer, A.C., 2021. A feasibility trial of gamma sensory flicker for patients with prodromal Alzheimer's disease. Alzheimer's & Dementia: Transl. Res. Clin. Intervent. 7, e12178.

Iaccarino, H.F., Singer, A.C., Martorell, A.J., Rudenko, A., Gao, F., Gillingham, T.Z., Mathys, H., Seo, J., Kritskiy, O., Abdurrob, F., Adaikkan, C., Canter, R.G., Rueda, R., Brown, E.N., Boyden, E.S., Tsai, L.-H., 2016. Gamma frequency entrainment attenuates amyloid load and modifies microglia. Nature 540, 230–235. https://doi.org/10.1038/nature20587.

Jack, C.R., Bennett, D.A., Blennow, K., Carrillo, M.C., Feldman, H.H., Frisoni, G.B., Hampel, H., Jagust, W.J., Johnson, K.A., Knopman, D.S., Petersen, R.C., Scheltens, P., Sperling, R.A., Dubois, B., 2016. A/T/N: An unbiased descriptive classification scheme for Alzheimer disease biomarkers. Neurology 87, 539–547. https://doi.org/10.1212/WNL.0000000000002923.

Ibáñez-Molina, A.J., Lozano, V., Soriano, M.F., Aznarte, J.I., Gómez-Ariza, C.J., Bajo, M. T., 2018. EEG Multiscale Complexity in Schizophrenia During Picture Naming. Front Physiol 9, 1213. https://doi.org/10.3389/fphys.2018.01213.

Jack, C.R., Bennett, D.A., Blennow, K., Carrillo, M.C., Dunn, B., Haeberlein, S.B., Holtzman, D.M., Jagust, W., Jessen, F., Karlawish, J., Liu, E., Molinuevo, J.L., Montine, T., Phelps, C., Rankin, K.P., Rowe, C.C., Scheltens, P., Siemers, E., Snyder, H.M., Sperling, R., Contributors, 2018. NIA-AA Research Framework: Toward a biological definition of Alzheimer's disease. Alzheimers Dement. 14, 535–562. https://doi.org/10.1016/j.jalz.2018.02.018.

Jelic, V., Shigeta, M., Julin, P., Almkvist, O., Winblad, B., Wahlund, L.O., 1996. Quantitative electroencephalography power and coherence in Alzheimer's disease and mild cognitive impairment. Dementia 7, 314–323. https://doi.org/10.1159/000106897.

Jeong, H.T., Youn, Y.C., Sung, H.-H., Kim, S.Y., 2021. Power Spectral Changes of Quantitative EEG in the Subjective Cognitive Decline: Comparison of Community Normal Control Groups. Neuropsychiatr. Dis. Treat. 17, 2783–2790. https://doi.org/10.2147/NDT.S320130.

Jessen, F., Amariglio, R.E., Buckley, R.F., van der Flier, W.M., Han, Y., Molinuevo, J.L., Rabin, L., Rentz, D.M., Rodriguez-Gomez, O., Saykin, A.J., Sikkes, S.A.M., Smart, C. M., Wolfsgruber, S., Wagner, M., 2020. The characterisation of subjective cognitive decline. Lancet Neurol. 19, 271–278.

Jessen, F., Amariglio, R.E., van Boxtel, M., Breteler, M., Ceccaldi, M., Chételat, G., Dubois, B., Dufouil, C., Ellis, K.A., van der Flier, W.M., Glodzik, L., van Harten, A.C., de Leon, M.J., McHugh, P., Mielke, M.M., Molinuevo, J.L., Mosconi, L., Osorio, R.S., Perrotin, A., Petersen, R.C., Rabin, L.A., Rami, L., Reisberg, B., Rentz, D.M., Sachdev, P.S., de la Sayette, V., Saykin, A.J., Scheltens, P., Shulman, M.B., Slavin, M.J., Sperling, R.A., Stewart, R., Uspenskaya, O., Vellas, B., Visser, P.J., Wagner, M., Group, S.C.D.I. (SCD-I.W., 2014. A conceptual framework for research on subjective cognitive decline in preclinical Alzheimer's disease. Alzheimer's Dement. 10, 844–852.

Kikuchi, M., Koenig, T., Munesue, T., Hanaoka, A., Strik, W., Dierks, T., Koshino, Y., Minabe, Y., 2011. EEG microstate analysis in drug-naive patients with panic disorder. PLoS One 6, e22912. https://doi.org/10.1371/journal.pone.0022912.

Kim, J.-S., Lee, S.-H., Park, G., Kim, S., Bae, S.-M., Kim, D.-W., Im, C.-H., 2012. Clinical Implications of Quantitative Electroencephalography and Current Source Density in Patients with Alzheimer's Disease. Brain Topogr. 25, 461–474. https://doi.org/10.1007/s10548-012-0234-1.

Koenig, T., Melie-García, L., 2009. Statistical analysis of multichannel scalp field data. In: Michel, C.M., Brandeis, D., Wackermann, J., Gianotti, L.R.R., Koenig, T. (Eds.), Electrical Neuroimaging. Cambridge University Press, Cambridge, pp. 169–190. https://doi.org/10.1017/CBO9780511596889.009.

Koenig, T., Prichep, L., Lehmann, D., Sosa, P.V., Braeker, E., Kleinlogel, H., Isenhart, R., John, E.R., 2002. Millisecond by Millisecond, Year by Year: Normative EEG Microstates and Developmental Stages. Neuroimage 16, 41–48. https://doi.org/10.1006/nimg.2002.1070.

Koenig, T., Stein, M., Grieder, M., Kottlow, M., 2014. A Tutorial on Data-Driven Methods for Statistically Assessing ERP Topographies. Brain Topogr. 27, 72–83. https://doi.org/10.1007/s10548-013-0310-1.

Kulkarni, Nilesh, N., Parhad, Saurabh, V., Shaikh, Yasmin, P., 2017. Use of Non-linear and Complexity Features for EEG Based Dementia & Alzheimer Disease Diagnosis. In: 2017 International Conference on Computing, Communication, Control and Automation (ICCUBEA). Presented at the 2017 International Conference on Computing, Communication, Control and Automation (ICCUBEA), pp. 1–3. https://doi.org/10.1109/ICCUBEA.2017.8463870.

Lam, A.D., Shafi, M.M., 2022. Towards a coherent view of network hyperexcitability in Alzheimer's disease. Brain 145, 423–425. https://doi.org/10.1093/brain/awac033.

Lawton, M.P., Brody, E.M., 1969. Assessment of Older People: Self-Maintaining and Instrumental Activities of Daily Living. Gerontologist 9, 179–186. https://doi.org/10.1093/geront/9.3_Part_1.179.

Lazarou, I., Nikolopoulos, S., Dimitriadis (Yiannis), S.I., Kompatsiaris, I., Spilioti, M., Tsolaki, M., 2019. Is brain connectome research the future frontier for subjective cognitive decline? A systematic review. Clin. Neurophysiol. 130, 1762–1780. https://doi.org/10.1016/j.clinph.2019.07.004.

Lazarou, I., Georgiadis, K., Nikolopoulos, S., Oikonomou, V.P., Tsolaki, A., Kompatsiaris, I., Tsolaki, M., Kugiumtzis, D., 2020. A novel connectome-based electrophysiological study of subjective cognitive decline related to Alzheimer's disease by using resting-state high-density EEG EGI GES 300. Brain Sci. 10, 1–29. https://doi.org/10.3390/brainsci10060392.

Li, J., Li, N., Shao, X., Chen, J., Hao, Y., Li, X., Hu, B., 2021. Altered Brain Dynamics and Their Ability for Major Depression Detection using EEG Microstates Analysis. IEEE Transactions on Affective Computing, 1–1. https://doi.org/10.1109/TAFFC.2021.3139104.

López-Sanz, D., Bruña, R., Garcés, P., Camara, C., Serrano, N., Rodríguez-Rojo, I.C., Delgado, M.L., Montenegro, M., López-Higes, R., Yus, M., Maestú, F., 2016. Alpha band disruption in the AD-continuum starts in the Subjective Cognitive Decline stage: a MEG study. Sci. Rep. 6, 37685. https://doi.org/10.1038/srep37685.

López-Sanz, D., Bruña, R., Garcés, P., Martín-Buro, M.C., Walter, S., Delgado, M.L., Montenegro, M., López Higes, R., Marcos, A., Maestú, F., 2017. Functional Connectivity Disruption in Subjective Cognitive Decline and Mild Cognitive Impairment: A Common Pattern of Alterations. Front. Aging Neurosci. 9, 109. https://doi.org/10.3389/fnagi.2017.00109.

Maestú, F., Cuesta, P., Hasan, O., Fernandéz, A., Funke, M., Schulz, P.E., 2019. The Importance of the Validation of M/EEG With Current Biomarkers in Alzheimer's Disease. Front. Hum. Neurosci. 13, 17. https://doi.org/10.3389/fnhum.2019.00017.

Mahjoory, K., Nikulin, V.V., Botrel, L., Linkenkaer-Hansen, K., Fato, M.M., Haufe, S., 2017. Consistency of EEG source localization and connectivity estimates. Neuroimage 152, 590–601. https://doi.org/10.1016/j.neuroimage.2017.02.076.

Malek, N., Baker, M.R., Mann, C., Greene, J., 2017. Electroencephalographic markers in dementia. Acta Neurol. Scand. 135, 388–393. https://doi.org/10.1111/ane.12638.

Margolis, S.A., Kelly, D.A., Daiello, L.A., Davis, J., Tremont, G., Pillemer, S., Denby, C., Ott, B.R., 2020. Anticholinergic/Sedative Drug Burden and Subjective Cognitive Decline in Older Adults at Risk of Alzheimer's Disease. J. Gerontol.: Ser. A. https://doi.org/10.1093/gerona/glaa222.

Maslov, S., Sneppen, K., 2002. Specificity and stability in topology of protein networks. Science 296, 910–913. https://doi.org/10.1126/science.1065103.

Mazzeo, S., Bessi, V., Padiglioni, S., Bagnoli, S., Bracco, L., Sorbi, S., Nacmias, B., 2019a. KIBRA T allele influences memory performance and progression of cognitive decline: a 7-year follow-up study in subjective cognitive decline and mild cognitive impairment. Neurol. Sci. https://doi.org/10.1007/s10072-019-03866-8.

Mazzeo, S., Lassi, M., Padiglioni, S., Vergani, A.A., Moschini, V., Scarpino, M., Giacomucci, G., Burali, R., Morinelli, C., Fabbiani, C., Galdo, G., Bagnoli, S., Emiliani, F., Ingannato, A., Nacmias, B., Sorbi, S., Grippo, A., Mazzoni, A., Bessi, V.. PRedicting the EVolution of SubjectIvE Cognitive Decline to Alzheimer's Disease With machine learning: the PREVIEW study protocol. https://doi.org/10.1101/2023.04.15.23288619.

Mazzeo, S., Padiglioni, S., Bagnoli, S., Bracco, L., Nacmias, B., Sorbi, S., Bessi, V., 2019b. The dual role of cognitive reserve in subjective cognitive decline and mild cognitive impairment: a 7-year follow-up study. J. Neurol. 266, 487–497. https://doi.org/10.1007/s00415-018-9164-5.

Mazzeo, S., Padiglioni, S., Bagnoli, S., Carraro, M., Piaceri, I., Bracco, L., Nacmias, B., Sorbi, S., Bessi, V., 2020. Assessing the effectiveness of subjective cognitive decline

plus criteria in predicting the progression to Alzheimer's disease: an 11-year follow-up study. Eur. J. Neurol. 27, 894–899. https://doi.org/10.1111/ene.14167.
Mazzeo, S., Bessi, V., Bagnoli, S., Giacomucci, G., Balestrini, J., Padiglioni, S., Tomaiuolo, G., Ingannato, A., Ferrari, C., Bracco, L., Sorbi, S., Nacmias, B., 2021. Dual Effect of PER2 C111G Polymorphism on Cognitive Functions across Progression from Subjective Cognitive Decline to Mild Cognitive Impairment. Diagnostics (Basel) 11, 718. https://doi.org/10.3390/diagnostics11040718.
Mazzeo, S., Emiliani, F., Bagnoli, S., Padiglioni, S., Conti, V., Ingannato, A., Giacomucci, G., Balestrini, J., Ferrari, C., Sorbi, S., Nacmias, B., Bessi, V., 2022. Huntingtin gene intermediate alleles influence the progression from subjective cognitive decline to mild cognitive impairment: A 14-year follow-up study. Eur. J. Neurol. 29, 1600–1609. https://doi.org/10.1111/ene.15291.
McKhann, G.M., Knopman, D.S., Chertkow, H., Hyman, B.T., Jack, C.R., Kawas, C.H., Klunk, W.E., Koroshetz, W.J., Manly, J.J., Mayeux, R., Mohs, R.C., Morris, J.C., Rossor, M.N., Scheltens, P., Carrillo, M.C., Thies, B., Weintraub, S., Phelps, C.H., 2011. The diagnosis of dementia due to Alzheimer's disease: recommendations from the National Institute on Aging-Alzheimer's Association workgroups on diagnostic guidelines for Alzheimer's disease. Alzheimers Dement. 7, 263–269. https://doi.org/10.1016/j.jalz.2011.03.005.
Meghdadi, A.H., Karić, M.S., McConnell, M., Rupp, G., Richard, C., Hamilton, J., Salat, D., Berka, C., 2021. Resting state EEG biomarkers of cognitive decline associated with Alzheimer's disease and mild cognitive impairment. PLoS One 16, e0244180.
Michel, C.M., Koenig, T., 2018. EEG microstates as a tool for studying the temporal dynamics of whole-brain neuronal networks: a review. NeuroImage Brain Connectivity Dyn. 180, 577–593.
Milz, P., Faber, P.L., Lehmann, D., Koenig, T., Kochi, K., Pascual-Marqui, R.D., 2016. The functional significance of EEG microstates—associations with modalities of thinking. Neuroimage 125, 643–656.
Murphy, M., Wang, J., Jiang, C., Wang, L., Kozhemiako, N., Wang, Y., Consortium, the G., Pan, J.Q., Purcell, S.M., 2022. Bias in group-level EEG microstate analysis. https://doi.org/10.1101/2022.11.07.515464.
Murphy, M., Whitton, A.E., Deccy, S., Ironside, M.L., Rutherford, A., Beltzer, M., Sacchet, M., Pizzagalli, D.A., 2020. Abnormalities in electroencephalographic microstates are state and trait markers of major depressive disorder. Neuropsychopharmacology 45, 2030–2037. https://doi.org/10.1038/s41386-020-0749-1.
Murray, M.M., Brunet, D., Michel, C.M., 2008. Topographic ERP analyses: A step-by-step tutorial review.
Musaeus, C.S., Engedal, K., Høgh, P., Jelic, V., Khanna, A.R., Kjær, T.W., Mørup, M., Naik, M., Oeksengaard, A.-R., Santarnecchi, E., Snaedal, J., Wahlund, L.-O., Waldemar, G., Andersen, B.B., 2020. Changes in the left temporal microstate are a sign of cognitive decline in patients with Alzheimer's disease. Brain Behav. 10, e01630.
Nishida, K., Morishima, Y., Yoshimura, M., Isotani, T., Irisawa, S., Jann, K., Dierks, T., Strik, W., Kinoshita, T., Koenig, T., 2013. EEG microstates associated with salience and frontoparietal networks in frontotemporal dementia, schizophrenia and Alzheimer's disease. Clin. Neurophysiol. 124, 1106–1114. https://doi.org/10.1016/j.clinph.2013.01.005.
Nolte, G., Bai, O., Wheaton, L., Mari, Z., Vorbach, S., Hallett, M., 2004. Identifying true brain interaction from EEG data using the imaginary part of coherency. Clin. Neurophysiol. 115, 2292–2307. https://doi.org/10.1016/j.clinph.2004.04.029.
Oostenveld, R., Praamstra, P., 2001. The five percent electrode system for high-resolution EEG and ERP measurements. Clin. Neurophysiol. 112, 713–719. https://doi.org/10.1016/S1388-2457(00)00527-7.
Oostenveld, R., Stegeman, D.F., Praamstra, P., van Oosterom, A., 2003. Brain symmetry and topographic analysis of lateralized event-related potentials. Clin. Neurophysiol. 114, 1194–1202. https://doi.org/10.1016/S1388-2457(03)00059-2.
Oostenveld, R., Fries, P., Maris, E., Schoffelen, J.-M., 2011. FieldTrip: Open source software for advanced analysis of MEG, EEG, and invasive electrophysiological data. Comput. Intell. Neurosci. 2011, 156869. https://doi.org/10.1155/2011/156869.
Pascual-Marqui, R.D., Michel, C.M., Lehmann, D., 1995. Segmentation of Brain Electrical Activity into Microstates; Model Estimation and Validation. IEEE Trans. Biomed. Eng. 42, 658–665. https://doi.org/10.1109/10.391164.
Pascual-Marqui, R.D., 2007. Discrete, 3D distributed, linear imaging methods of electric neuronal activity. Part 1: exact, zero error localization. arXiv:0710.3341 [math-ph, physics:physics, q-bio].
Perrotin, A., Mormino, E.C., Madison, C.M., Hayenga, A.O., Jagust, W.J., 2012. Subjective Cognition and Amyloid Deposition Imaging: A Pittsburgh Compound B Positron Emission Tomography Study in Normal Elderly Individuals. Arch. Neurol. 69, 223–229. https://doi.org/10.1001/archneurol.2011.666.
Petersen, R.C., 2004. Mild cognitive impairment as a diagnostic entity. J. Intern. Med. 256, 183–194. https://doi.org/10.1111/j.1365-2796.2004.01388.x.
Pion-Tonachini, L., Kreutz-Delgado, K., Makeig, S., 2019. ICLabel: An automated electroencephalographic independent component classifier, dataset, and website. Neuroimage 198, 181–197. https://doi.org/10.1016/j.neuroimage.2019.05.026.
Poulsen, A.T., Pedroni, A., Langer, N., Hansen, L.K., 2018. Microstate EEGlab toolbox: An introductory guide.
Rempe, M.P., Ott, L.R., Picci, G., Penhale, S.H., Christopher-Hayes, N.J., Lew, B.J., Petro, N.M., Embury, C.M., Schantell, M., Johnson, H.J., Okelberry, H.J., Losh, K.L., Willett, M.P., Losh, R.A., Wang, Y.-P., Calhoun, V.D., Stephen, J.M., Heinrichs-Graham, E., Kurz, M.J., Wilson, T.W., 2023. Spontaneous cortical dynamics from the first years to the golden years. Proceedings of the National Academy of Sciences 120, e2212776120. https://doi.org/10.1073/pnas.2212776120.
Rossini, P.M., Del Percio, C., Pasqualetti, P., Cassetta, E., Binetti, G., Dal Forno, G., Ferreri, F., Frisoni, G., Chiovenda, P., Miniussi, C., Parisi, L., Tombini, M., Vecchio, F., Babiloni, C., 2006. Conversion from mild cognitive impairment to Alzheimer's disease is predicted by sources and coherence of brain electroencephalography rhythms. Neuroscience 143, 793–803. https://doi.org/10.1016/j.neuroscience.2006.08.049.
Rossini, P.M., Miraglia, F., Alù, F., Cotelli, M., Ferreri, F., Iorio, R.D., Iodice, F., Vecchio, F., 2020. Neurophysiological Hallmarks of Neurodegenerative Cognitive Decline: The Study of Brain Connectivity as A Biomarker of Early Dementia. J. Personalized Med. 10, 34. https://doi.org/10.3390/jpm10020034.
Rubinov, M., Sporns, O., 2010. Complex network measures of brain connectivity: Uses and interpretations. NeuroImage Comput. Models Brain 52, 1059–1069. https://doi.org/10.1016/j.neuroimage.2009.10.003.
Shumbayawonda, E., López-Sanz, D., Bruña, R., Serrano, N., Fernández, A., Maestú, F., Abasolo, D., 2020. Complexity changes in preclinical Alzheimer's disease: An MEG study of subjective cognitive decline and mild cognitive impairment. Clin. Neurophysiol. 131, 437–445. https://doi.org/10.1016/j.clinph.2019.11.023.
Silva, D., Guerreiro, M., Maroco, J., Santana, I., Rodrigues, A., Bravo Marques, J., de Mendonça, A., 2012. Comparison of four verbal memory tests for the diagnosis and predictive value of mild cognitive impairment. Dement. Geriatr. Cogn. Dis. Extra 2, 120–131. https://doi.org/10.1159/000336224.
Smailovic, U., Koenig, T., Kåreholt, I., Andersson, T., Kramberger, M.G., Winblad, B., Jelic, V., 2018. Quantitative EEG power and synchronization correlate with Alzheimer's disease CSF biomarkers. Neurobiol. Aging 63, 88–95.
Smailovic, U., Koenig, T., Laukka, E.J., Kalpouzos, G., Andersson, T., Winblad, B., Jelic, V., 2019. EEG time signature in Alzheimer's disease: Functional brain networks falling apart. NeuroImage: Clin. 24, 102046. https://doi.org/10.1016/j.nicl.2019.102046.
Smailovic, U., Koenig, T., Savitcheva, I., Chiotis, K., Nordberg, A., Blennow, K., Winblad, B., Jelic, V., 2020. Regional Disconnection in Alzheimer Dementia and Amyloid-Positive Mild Cognitive Impairment: Association Between EEG Functional Connectivity and Brain Glucose Metabolism. Brain Connect. 10, 555–565. https://doi.org/10.1089/brain.2020.0785.
Sperling, R.A., Aisen, P.S., Beckett, L.A., Bennett, D.A., Craft, S., Fagan, A.M., Iwatsubo, T., Jack, C.R., Kaye, J., Montine, T.J., Park, D.C., Reiman, E.M., Rowe, C. C., Siemers, E., Stern, Y., Yaffe, K., Carrillo, M.C., Thies, B., Morrison-Bogorad, M., Wagster, M.V., Phelps, C.H., 2011. Toward defining the preclinical stages of Alzheimer's disease: Recommendations from the National Institute on Aging-Alzheimer's Association workgroups on diagnostic guidelines for Alzheimer's disease. Alzheimers Dement. 7, 280–292. https://doi.org/10.1016/j.jalz.2011.03.003.
Sporns, O., Zwi, J.D., 2004. The small world of the cerebral cortex. Neuroinformatics 2, 145–162. https://doi.org/10.1385/NI:2:2:145.
Stewart, R., Godin, O., Crivello, F., Maillard, P., Mazoyer, B., Tzourio, C., Dufouil, C., 2011. Longitudinal neuroimaging correlates of subjective memory impairment: 4-year prospective community study. Br. J. Psychiatry 198, 199–205. https://doi.org/10.1192/bjp.bp.110.078683.
Tait, L., Tamagnini, F., Stothart, G., Barvas, E., Monaldini, C., Frusciante, R., Volpini, M., Guttmann, S., Coulthard, E., Brown, J.T., Kazanina, N., Goodfellow, M., 2020. EEG microstate complexity for aiding early diagnosis of Alzheimer's disease. Sci. Rep. 10.
Tait, L., Zhang, J., 2022. +microstate: A MATLAB toolbox for brain microstate analysis in sensor and cortical EEG/MEG. Neuroimage 258, 119346. https://doi.org/10.1016/j.neuroimage.2022.119346.
Tzourio-Mazoyer, N., Landeau, B., Papathanassiou, D., Crivello, F., Etard, O., Delcroix, N., Mazoyer, B., Joliot, M., 2002. Automated anatomical labeling of activations in SPM using a macroscopic anatomical parcellation of the MNI MRI single-subject brain. Neuroimage 15, 273–289. https://doi.org/10.1006/nimg.2001.0978.
Van de Ville, D., Britz, J., Michel, C.M., 2010. EEG microstate sequences in healthy humans at rest reveal scale-free dynamics. PNAS 107, 18179–18184. https://doi.org/10.1073/pnas.1007841107.
Vecchio, F., Miraglia, F., Iberite, F., Lacidogna, G., Guglielmi, V., Marra, C., Pasqualetti, P., Tiziano, F.D., Rossini, P.M., 2018. Sustainable method for Alzheimer dementia prediction in mild cognitive impairment: electroencephalographic connectivity and graph theory combined with apolipoprotein E. Ann. Neurol. 84, 302–314. https://doi.org/10.1002/ana.25289.
Vellas, B., Aisen, P.S., Sampaio, C., Carrillo, M., Scheltens, P., Scherrer, B., Frisoni, G.B., Weiner, M., Schneider, L., Gauthier, S., Gispen-de Wied, C.C., Hendrix, S., Feldman, H., Cedarbaum, J., Petersen, R., Siemers, E., Andrieu, S., Prvulovic, D., Touchon, J., Hampel, H., 2011. Prevention trials in Alzheimer's disease: an EU-US task force report. Prog. Neurobiol. 95, 594–600. https://doi.org/10.1016/j.pneurobio.2011.08.014.
von Wegner, F., Knaut, P., Laufs, H., 2018. EEG Microstate Sequences From Different Clustering Algorithms Are Information-Theoretically Invariant. Frontiers in Computational Neuroscience 12.
Wang, X., Huang, W., Su, L., Xing, Y., Jessen, F., Sun, Y., Shu, N., Han, Y., 2020. Neuroimaging advances regarding subjective cognitive decline in preclinical Alzheimer's disease. Mol. Neurodegener. 15, 55. https://doi.org/10.1186/s13024-020-00395-3.
Wolfsgruber, S., Kleineidam, L., Guski, J., Polcher, A., Frommann, I., Roeske, S., Spruth, E.J., Franke, C., Priller, J., Kilimann, I., Teipel, S., Buerger, K., Janowitz, D., Laske, C., Buchmann, M., Peters, O., Menne, F., Fuentes Casan, M., Wiltfang, J., Bartels, C., Düzel, E., Metzger, C., Glanz, W., Thelen, M., Spottke, A., Ramirez, A., Kofler, B., Fließbach, K., Schneider, A., Heneka, M.T., Brosseron, F., Meiberth, D., Jessen, F., Wagner, M., DELCODE Study Group, 2020. Minor neuropsychological deficits in patients with subjective cognitive decline. Neurology 95, e1134–e1143. https://doi.org/10.1212/WNL.0000000000010142.

Xu, X., Li, W., Tao, M., Xie, Z., Gao, X., Yue, L., Wang, P., 2020. Effective and Accurate Diagnosis of Subjective Cognitive Decline Based on Functional Connection and Graph Theory View. Front. Neurosci. 14, 577887. https://doi.org/10.3389/fnins.2020.577887.

Zappasodi, F., Croce, P., Giordani, A., Assenza, G., Giannantoni, N.M., Profice, P., Granata, G., Rossini, P.M., Tecchio, F., 2017. Prognostic Value of EEG Microstates in Acute Stroke. Brain Topography 2017 30:5 30, 698–710. https://doi.org/10.1007/S10548-017-0572-0.

Zappasodi, F., Marzetti, L., Olejarczyk, E., Tecchio, F., Pizzella, V., 2015. Age-Related Changes in Electroencephalographic Signal Complexity. PLoS One 10, e0141995. https://doi.org/10.1371/journal.pone.0141995.

Zhang, Y., Zhang, Z., Luo, L., Tong, H., Chen, F., Hou, S.-T., 2021. 40 Hz Light Flicker Alters Human Brain Electroencephalography Microstates and Complexity Implicated in Brain Diseases. Front. Neurosci. 15.